I&EC research
Industrial & Engineering Chemistry Research

Article

Cite This: Ind. Eng. Chem. Res. 2018, 57, 2050−2067

pubs.acs.org/IECR

Sibunit-Supported Mono- and Bimetallic Catalysts Used in Aqueous-Phase Reforming of Xylitol

Lidia I. Godina,[†] Alexey V. Kirilin,[§,†] Anton V. Tokarev,[†] Irina L. Simakova,[‡] and Dmitry Yu. Murzin*[,†]

[†]Laboratory of Industrial Chemistry and Reaction Engineering, Process Chemistry Centre, Åbo Akademi University, FI-20500 Turku, Finland

[‡]Boreskov Institute of Catalysis, pr. Lavrentieva 5, Novosibirsk 630090, Russia

Supporting Information

ABSTRACT: Carbon-supported mono- and bimetallic catalysts prepared via incipient wetness impregnation were systematically studied in aqueous-phase reforming (APR) of xylitol aiming at hydrogen production from biomass. The catalytic performance of several VIII group metals and their combinations, such as Pt, Ni, Pt−Ni, Re, Pt−Re, Ru, Pt−Ru, and Pt−Co, was compared for xylitol APR in a fixed-bed reactor at 225 °C and 29.7 bar (N_2). Ni/C, Ru/C, and Re/C catalysts displayed significantly lower activity compared to others. Activity and selectivity to H_2 of bimetallic Pt−Ni/C, Pt−Co/C, and Pt−Ru/C catalysts were close to that of Pt/C. Pt−Re/C catalyst showed an outstanding performance which was accompanied by a shift of the reaction pathways to the alkane formation and thereby lower hydrogen selectivity. Addition of the second metal to Pt was not found to be beneficial for hydrogen production, thus leaving Pt/C as the optimum carbon-supported catalyst.

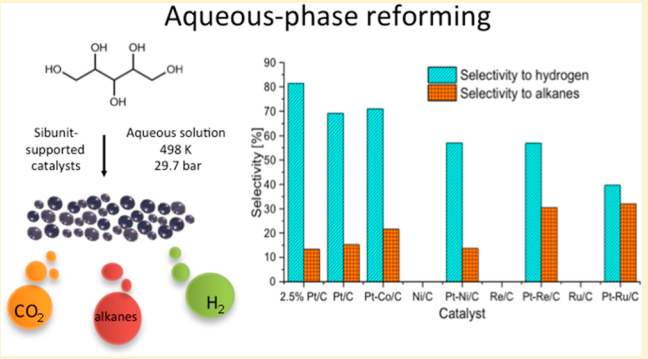

1. INTRODUCTION

Hydrogen production from renewable biomass sources is possible via a promising aqueous-phase reforming (APR) process. Liquid-phase reforming of different organic molecules with hydroxyl groups occurs on transition metals already at relatively low temperatures (463−523 K), which makes it more energy-efficient than steam reforming.[1] Biomass conversion requires catalysts with high hydrothermal stability and resistance to impurities presented in the feedstock. The main task of this study is development of a catalyst able to possess stable properties and high activity during a prolonged hydrothermal treatment.

Various supports have been explored in APR, including different carbon materials. Among such supports, a mesoporous carbonaceous material Sibunit is considered as an attractive one because of high mechanical crushing and abrasion strength (up to 200−300 kg/cm^2) and high surface area (up to 700 m^2/g).[2] It combines the properties of graphite and activated carbon. Sibunit catalysts can in principle be produced in a large scale in a number of shape units, such as whole and hollow cylinders, rings, etc., allowing their application in fixed bed reactors. The carbon material is synthesized via deposition of pyrolytic carbon from C_1−C_3 hydrocarbons on granulated carbon blacks followed by chemical vapor deposition and steam activation. A detailed preparation procedure is described by Fenelonov et al.[3]

Activity and selectivity in APR can be adjusted by tuning process and catalyst parameters, such as active metal, type of support, and the reaction conditions (pressure, temperature, addition of acids/bases, presence of the carrier gas, reactor type). The impact of the catalyst choice and operation conditions is discussed below.

1.1. Influence of Process Conditions on Product Distribution. Neira D'Angelo et al.[4] showed that mass-transfer of hydrogen has a large impact on product selectivity. Even if this was shown for the APR of sorbitol in a microchannel reactor, it should be taken as a general rule rather than an exception. The same authors provided an extensive description of tunable parameters influence for a three-phase reactor model.[5] The most important parameter was hydrogen pressure, which exhibited a pronounced negative effect on the reforming rate. Hydrogen produced during APR can be consumed again in hydrogenation−hydrogenolysis reactions, e.g., for alkane production. Thus, the reactor type, and especially the degree of back-mixing, will also determine the hydrogen to alkane ratio.[4−6] Hydrogen can be removed from the reaction zone using a reactive-separation approach in membrane reactors,[7] or hypothetically in a semibatch reactor with an inert quenching. Moreover, dilution of hydrogen can be achieved to a certain extent in continuous reactors with a constant flow of a carrier gas. Thus, comparison of results in the literature should be

Received: November 28, 2017
Revised: January 13, 2018
Accepted: January 25, 2018
Published: January 25, 2018

DOI: 10.1021/acs.iecr.7b04937
Ind. Eng. Chem. Res. 2018, 57, 2050−2067

Table 1. Carbon-Supported Catalysts Used for APR

metal	reactor	feed and reference
Pt/C	autoclave	methanol,[25] ethylene glycol,[20,26] glycerol,[27−31] sorbitol,[22] glucose,[19,22,32] cellulose,[22,33] syringol;[25] guaiacol,[25] catechol,[25] phenol,[25] wheat straw hydrolysate,[19,34,35] kenaf hydrolysate,[36] ethylene glycol + KOH,[37] glycerol + CaO (sorption enhanced)[18]
	ceramic membrane reactor	sorbitol[7]
	fixed bed	ethylene glycol,[23,38−45] glycerol,[44−49] propylene glycol,[44] xylitol,[49,50] sorbitol,[44,51,52] ethylene glycol + KOH[37]
	semibatch	crude glycerol[53]
	single-channel microreactor	glycerol,[44] glycerol + KOH[55]
Re/C	autoclave	glycerol[27,56]
	fixed bed	ethylene glycol[44]
Pt−Re/C	autoclave	ethanol,[57] glycerol,[27,29,30,56] formic acid,[57] acetaldehyde,[57] acetic acid,[57] waste lipids[58]
	fixed bed	ethylene glycol,[23,44] glycerol,[44,46] propylene glycol[44]
	single-channel microreactor	glycerol,[54] glycerol + KOH[55]
Ru/C	autoclave	wheat straw hydrolysate[34]
	fixed bed	sorbitol,[6,51] acetic acid[59]
Pt−Ru/C	fixed bed	sorbitol[51]
	autoclave	glucose,[19] cellulose,[33] wheat straw hydrolysate,[19] glycerol + CaO (sorption enhanced)[18]
Ni/C	autoclave	methanol,[25] ethylene glycol,[20] syringol,[25] guaiacol,[25] catechol,[25] phenol,[25] cellulose,[22] glucose,[22] ethylene glycol + KOH,[37] sorbitol + $Ba(OH)_2$[24]
	fixed bed	glycerol,[60] ethylene glycol + KOH[37]
Pt−Ni/C	autoclave	glucose,[19] wheat straw hydrolysate,[19] glycerol + CaO (sorption enhanced)[18]
Pt−Co/C	autoclave	glycerol,[48,61] glycerol + CaO (sorption enhanced)[18]
	fixed bed	ethylene glycol[38,39,42]

done with care considering the reactor type used for generation of experimental data.

Another comprehensive study on variable conditions influencing APR was performed by Roy et al.[8] for *n*-butanol reforming over Ni/CeO_2 and Ni/Al_2O_3 catalysts. Selectivity to hydrogen and CO_2 exhibited a maximim at an optimal pressure at a bubble point region.

There are other parameters that influence products selectivity as well. Duarte et al.[9,10] recently published a comprehensive study on the influence of metal loading and the feed type. The metal loading was shown to have a clear impact on hydrogen selectivity and even on the distribution of carbon between the liquid- and gas-phase products. Variations of the feed concentration together with the catalyst loading was performed by Serets and Tsiarakas.[11] Changes in concentration influenced distribution of the liquid-phase products and selectivity to methane in the APR of crude glycerol over 65% Ni/SiO_2−Al_2O_3 catalyst. The effects of temperature, pressure, feed concentration, and the ratio of the catalyst mass to the glycerol mass flow were studied by Remón et al.[12] for the APR of partially purified crude glycerol over Pt/Al_2O_3 catalyst. The results indicated that the product distribution is significantly affected by the operation variables.

1.2. Influence of Active Metal and Support. Various transition and especially noble metals are active in APR. Moreover, metalloids, e.g. boron,[13] or specific materials like graphene[14] were shown to be active in glycerol reforming. A broad metal screening was performed for catalysts supported on alumina,[15] titania,[16] silica,[17] carbon multiwalled nanotubes,[18,19] carbon nanofibers,[20] carbon black,[21] and activated carbon.[22−24] Pt was shown to have high activity and selectivity to hydrogen in most cases. Both parameters could be improved via an addition of a second transition metal, like Ni or Co. A summary of various studies on carbon-supported catalysts for APR of different feedstock is presented in Table 1.

Monometallic Ni and Co catalysts are known to be unstable at the APR conditions because of leaching issues.[20,37] Several studies were devoted to investigation of Ni (or Pt−Ni) catalysts in APR with mostly metal oxides used as supports.[62] The results vary significantly depending on the support and reactor type. Deactivation, including coking, leaching of the active metal, or oxidation for Ni-containing catalysts, is described in several reports.[47,63−66] In a series of reports it was suggested to combine hydrogenation ability of Ni with highly acidic zeolite supports to obtain high selectivity toward alkanes with a high molar mass, e.g., pentane from xylitol.[67,68]

Bimetallic Pt−Ni and Pt−Co carbon-supported catalysts were shown to have better activity compared to monometallic Pt.[18,38] However, stability of Pt−Co/C is an issue because of high formation rates of acids and hence corresponding low pH which facilitates cobalt leaching.[48,61] Stability of Pt−Ni carbon supported catalyst was discussed for the sorption-enhanced APR of glycerol.[18]

Addition of Co to Pt (molar ratio 1:1) increased the reaction site-time yields by a factor of 2 for the APR of glycerol as shown by Dietrich et al.[61] for carbon nanotubes as the support. The conversion level of glycerol was chosen in the range of 2−4% for operation in a differential reactor mode, which makes it challenging to compare the results with the majority of other literature data and the current work. Pt−Co catalysts on single-wall nanotubes (SWNT) had higher hydrogen yields than monometallic Pt under the same reaction conditions for the APR of ethylene glycol[38] and also higher conversion levels.[39]

Van Haasterecht et al.[20] performed the tests with Ni, as well as Co and Pt on carbon nanofibers in the APR of ethylene glycol in a batch reactor. Activity of the Ni catalyst (14.5% conversion) was slightly lower than that for Pt (17%). At the same time, selectivity to hydrogen was 53% for Pt, being approximately 2.5 times higher than that for Co (21%) and Ni (15%) because of high methane formation rates for the latter two metals. Significant leaching of Co occurred because of high

DOI: 10.1021/acs.iecr.7b04937
Ind. Eng. Chem. Res. 2018, 57, 2050−2067

concentrations of acids in the liquid phase; 8.9% of the metal was lost after 24 h. The nickel leaching rate was slower compared to Co (1.9% of the metal leached after 24 h). No leaching of Pt was detected (<0.1 ppmw). Deactivation of Pt and Ni catalysts was mainly explained by the metal particle sintering; however, in the case of Ni, deposition of coke also needs to be taken into account.[38]

Monometallic Re/C was reported to have a low activity in the APR of ethylene glycol[44] and glycerol.[56] Ru/C catalysts, however, were active in the APR of sorbitol performed in a washcoated microreactor. Nevertheless, hydrogen production rates were very low.[6,51]

Carbon-supported bimetallic Pt−Re/C catalysts showed an outstanding activity, shifting reaction pathways toward alkane formation.[23,29,30,54−56] Addition of Ru to Pt also increased catalyst activity in the APR of sorbitol.[51]

Reaction pathways strongly depend on the type of the support.[40,43,44] Lewis or Brønsted acid sites present on the support can catalyze a number of reactions, for instance, dehydration. Surface groups, polarity, and hydrophobicity play a crucial role in the product distribution.[43] Different support types were tested for the same active metal, mainly for Pt and Ni.[25,40,41,47,53,69−72] Such supports as Al_2O_3, TiO_2, and carbon exhibited the highest activity for the hydrogen production in the APR of ethylene glycol performed by Shabaker et al.[40] The effect of support basicity was studied by Wen et al.[47] and Guo et al.[72] in the APR of glycerol in a fixed bed reactor. The catalysts can be ranked in the following order based on their activity:

$$\mathrm{Pt/MgO} > \mathrm{Pt/Al_2O_3} > \mathrm{Pt/CeO_2} > \mathrm{Pt/TiO_2} > \mathrm{Pt/SiO_2} > \mathrm{Pt/HUSY\ (SiO_2{:}\ Al_2O_3 = 4.8)} > \mathrm{Pt/activated\ carbon} > \mathrm{Pt/SAPO\text{-}11\ (Si_{0.129}Al_{0.499}P_{0.397}O_2)}$$

However, the most active and selective to hydrogen Pt/MgO catalyst deactivated after 25 h of time-on-stream with formation of magnesium hydroxide and carbonate. Support basicity was found to be beneficial for conversion of carbon to the gas-phase products and formation of hydrogen; at the same time, low hydrothermal stability prevents the selection of many solid bases as catalyst supports.

Carbon supports were shown to have a high hydrothermal stability in APR conditions.[41,42] Different types of carbon supports were compared for Pt catalysts.[35,45,50,52] Sibunit-supported Pt catalyst was tested in the APR of xylitol[50] and exhibited moderate results in terms of hydrogen production compared to Pt supported on birch activated carbon (BAC) or TiC-derived carbon (TiC-CDC). However, it was more active than the above-mentioned catalysts. According to Kim et al.[41] and Kirilin et al.,[50] textural properties of the carbon support, such as porosity, as well as their acidity, have a strong influence on APR. Platinum supported on the ordered mesoporous carbon CMK-3 showed more than 2-fold higher hydrogen production compared to catalysts supported on activated carbon and alumina in the APR of ethylene glycol.[41] Those results were explained by an outstanding hydrothermal stability and open mesoporous structure of the support. The mesoporous carbon Sibunit therefore was chosen as a support material in the current study.

Sibunit-supported mono- and bimetallic catalysts, namely, Ni, Pt−Ni, Re, Pt−Re, Ru, Pt−Ru, and Pt−Co, were used for xylitol APR for the first time in the current study. This set of catalysts was compared in terms of activity and selectivity with a commercial Pt on active carbon and Sibunit-supported Pt/C.

2. EXPERIMENTAL SECTION

2.1. Catalyst Preparation. Mono- and bimetallic Pt, Ni, Pt−Ni, Re, Pt−Re, Ru, Pt−Ru, and Pt−Co catalysts were prepared by incipient wetness impregnation of the carbon support Sibunit with aqueous solution of corresponding metal precursors: H_2PtCl_6 (OAO Aurat, Russia), $RuCl_3{\cdot}nH_2O$ (Krastzvetmet, Russia), $HReO_4$ (20 wt %, Reachim, Russia), $CoCl_2{\cdot}3H_2O$ (Souzchimprom, Russia), $Ni(NO_3)_2{\cdot}nH_2O$ (Souzchimprom, Russia), and $NiCl_2{\cdot}nH_2O$ (Souzchimprom, Russia). The nominal metal loading of each metal was 3 wt %. The mass ratio was 1:1 for all bimetallic catalysts. The real metal loading was close to the nominal one, which was determined by XRF. The details can be found in Table 2. A commercial 2.5% Pt/C catalyst was provided by Johnson Matthey. The details of this catalyst characterization can be found elsewhere.[73]

Table 2. Mono- and Bimetallic Catalysts Used for the APR of Xylitol

catalyst	nominal content [wt %]	precursor	content determined by XRF [wt %]	temperatures during **reduction**/rereduction in situ [K]
2.5% Pt/C	2.5	$Pt(NO_3)_4$	2.5	n.a./523
Pt/C	3	H_2PtCl_6	2.9	**579**/523
Ni/C	3	$Ni(NO_3)_2$	n.m.	**613**/523
Re/C	3	$HReO_4$	2.9	**586**/623
Ru/C	3	$RuCl_3$	3.73	**627**/523
Pt−Ni/C	6/(3Pt:3Ni)[a]	H_2PtCl_6 + $Ni(NO_3)_2$	3.0 Pt:3.1 Ni	**613**/503
Pt−Re/C	6/(3Pt:3Re)[a]	H_2PtCl_6 + $HReO_4$	3.0 Pt:3.0 Re	**603**/523
Pt−Ru/C	6/(3Pt:3Ru)[a]	H_2PtCl_6 + $RuCl_3$	n.m.	**623**/523
Pt−Co/C	6/(3Pt:3Co)[a]	H_2PtCl_6 + $CoCl_2$	n.m.	**627**/523

[a]Bimetallic catalysts were prepared via coimpregnation.

Quartz fine granular from Merck KGaA was used for dilution of catalysts.

Additional treatment was applied to the support prior to impregnation. In particular, Sibunit was boiled in water for the dust removal and in an aqueous HCl (5 wt %) solution for removal of the metal impurities. The support was dried, sieved to obtain the desired particle size fraction (100−180 μm), and impregnated with the corresponding precursors.

After impregnation, the catalysts were dried overnight at 383 K and reduced in an excessive hydrogen flow (H_2, 40 mL/min) for 2−7 h. The reduction temperatures are listed in Table 2. All catalysts were rereduced in situ prior to catalytic experiments at the temperatures listed in the Table 2. Thermogravimetry−differential thermal analysis−mass spectrometry (TG-DTA-MS) studies of the unreduced samples were performed in order to determine the optimal reduction time and temperatures for each catalyst. The heating rate was 2 K/min.

Nitrates in the nitrate-based samples (Pt and Ni) were decomposed at 541 K in argon prior to reduction. Chloride-based samples were reduced up to 7 h in order to fully remove HCl. The $HReO_4$ catalyst required additional X-ray photoelectron spectroscopy (XPS) studies to determine the influence

DOI: 10.1021/acs.iecr.7b04937
Ind. Eng. Chem. Res. 2018, 57, 2050−2067

of the reduction conditions, such as the heating rate and the final reduction temperature, on formation of metallic Re.

2.2. Nitrogen Physisorption. The support was studied by nitrogen physisorption at 77 K on an ASAP-2400 (Micromeritics) instrument.

2.3. TEM. The size and the structure of metal particles were studied by transmission electron microscopy (TEM) on a JEM-2010 microscope (JEOL, Japan) with a lattice resolution of 0.14 nm at an accelerating voltage of 200 kV. Prior to TEM study, a sample was ground and suspended in ethanol. A drop of suspension was mounted on a copper grid coated with a holey carbon film, and the solvent was allowed to evaporate. The mean size of metal particles for each catalyst was determined by measuring the diameters (d_i) of over 350 particles which were seen in TEM micrographs taken with a medium magnification (e.g., 150 000−200 000 for particle size 3 nm). High-resolution (HR) imaging was carried out to determine the structure of the particles. The number of particles used in the calculation varied from 177 for Pt/C to 327 for Pt−Ru/C.

2.4. TG-DTA-MS. TG-DTA-MS analysis was performed on a Netzsch STA 409 PC equipped with a mass spectrometer SRS UGA 200. The measurements were carried out using corundum crucibles. DTA sample holder and the crucible were preheated to 1273 K in an air flow. Correction curves were recorded in accordance with the TPR experiment conditions from 323 to 1073 K with a temperature ramp of 10 K/min under argon, afterward in a mixture of argon and hydrogen (15% hydrogen in argon).

For TPR analysis, a series of catalysts samples was prepared when the synthesis was stopped before the reduction.

2.5. EDX. Local elemental analysis was performed using an energy-dispersive X-ray (EDX) spectroscopy using a Phoenix spectrometer (EDAX, United States) equipped with a Si(Li) detector giving the energy resolution of 130 eV. EDX analysis was used for determination of metal particle composition of Pt−Ni catalyst. EDX line scan data were collected from the particles lying on the support away from the others with the probe diameter of about 20 nm. Quantitative EDX measurements were carried out, for example, using the Pd Lα line, which does not overlap with the other X-ray emission lines.

2.6. XPS. XPS spectra were recorded using a SPECS spectrometer with PHOIBOS-150-MCD-9 hemispherical energy analyzer and X-ray monochromator FOCUS-500 (Al Kα irradiation, $h\upsilon$ = 1486.74 eV, 200 W). Binding energy scale was preliminarily calibrated by the position of the peaks of Au 4f7/2 (84.0 eV) and Cu 2p3/2 (932.67 eV) core levels. The binding energy (BE) and a full width at half-maximum (fwhm) are reported with the accuracy of 0.1 eV. The XPS spectra of the studied samples were compared to XPS-spectra of the reference samples. The ratios of surface atomic concentrations of the elements were calculated from the integral intensities of photoelectron peaks corrected by the corresponding atomic sensitivity factors (ASF).[74]

XPS studies were performed for Pt, Re, Ru, Pt−Ni, Pt−Ru, and Pt−Co catalysts. The influence of the reduction conditions, such as the heating rate and the final reduction temperature, was studied.

2.7. XRD. X-ray diffraction (XRD) patterns of Re/C catalyst was recorded with the X-ray diffractometer D8 (Bruker, Germany) using Cu K radiation and LynxEye detector by scanning with a step of 0.05° and an accumulation time of 3 s in each point with the slit width 0.26° or accumulation time of 1 s in each point with the slit width 0.52°.

2.8. XRF. Semiquantitative analysis of metal concentrations was performed using wavelength dispersive X-ray fluorescence (WDXRF) spectrometry with the powder pellet method. Undiluted samples (0.5 g) were milled and put in a 29 mm diameter die. The intensities of the metal lines in the samples were measured in vacuum conditions on an ARL Advant'X spectrometer equipped with a rhodium anode X-ray tube. Excitation conditions were as follows: tube voltage of 50 kV; current of 40 mA; collimator with a divergence of 0.25°; LiF200 crystal was used as a monochromator; scintillation counter was used as a detector; the counting time was 12 s. Contents of elements in the sample were estimated using a semiquantitative method by means of the QuantAS program for standardless analysis.

2.9. Ammonia Desorption. Acidity of the catalysts and the support was studied by NH_3 temperature-programmed desorption (TPD) on pulse chemisorption apparatus (Micromeritics, AutoChem 2900). The catalysts were dried at 373 K overnight prior to analysis. The samples (0.1 g) were loaded in a quartz U-tube and reduced in an excessive hydrogen flow (20 mL/min) at the temperature indicated in Table 2. The heating rate was 5 K/min, and the reduction time was 2 h. Thereafter, the catalyst was flushed with He (20 mL/min, 30 min) to remove hydrogen and cooled to the ambient temperature. Ammonia treatment with 5% NH_3 in He was performed for 1 h. Physically adsorbed ammonia was removed by He flow (20 mL/min, 30 min). The sample was heated to 498 K with the heating rates of 3, 5, 10, 15, or 20 K/min. After each heating step the sample was cooled to ambient temperature, flushed with He (20 mL/min, 15 min), and saturated with ammonia as described above.

Heat of desorption was calculated using a conventional approach plotting $1/T_p$ against $\ln(T^2/b)$, where T_p is temperature of the maximum desorption and b is heating rate, and determining the slope.[50]

2.10. Catalytic Experiments. The catalytic tests were performed in a downflow continuous lab-scale fixed-bed reactor. The experimental setup is shown in Figure 1. The

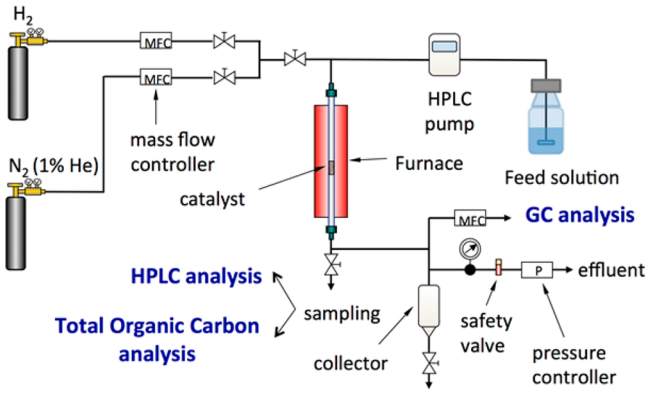

Figure 1. Experimental setup for aqueous phase reforming.

catalyst (0.5 g, mesh size 100−200 μm or powder in case of commercial 2.5% Pt/C) was diluted with quartz sand (1:1, mesh size 200−800 μm) and placed in the middle of a stainless-steel reactor tube between two layers of sand. The total catalytically active volume was 2.5 cm^3 and 3.8 cm^3 in the case of Sibunit-supported catalysts and commercial 2.5% Pt/C, respectively. The reactor was located in a furnace and connected to nitrogen (1% He) and hydrogen gas lines, the

DOI: 10.1021/acs.iecr.7b04937
Ind. Eng. Chem. Res. 2018, 57, 2050−2067

feed solution inlet, and the gas/liquid outlet line. An aqueous solution of xylitol (100 g in 1 L of water) was fed via a high-performance liquid chromatography (HPLC) pump. Gas−liquid separation took place in a T-shaped connector after cooling in a metal spring tube. There was no need for special cooling or any gas−liquid separating equipment because of constant nitrogen cofeeding (25 mL/min, STP) during the reaction. The liquid samples were periodically taken via a sampling loop for an offline HPLC analysis, while the gas samples were analyzed online by means of Micro-GC. Total organic carbon analysis of the liquid phase was carried out to control the carbon balance in all experiments except for those with Ni and Pt−Ni because of metal leaching.

The prereduced catalysts were additionally reduced in situ prior to the experiments in hydrogen flow (40 mL/min, STP). The following program was used: heating in a hydrogen flow from room temperature to 523−623 K with the rate of 5 K/min, dwelling for 2 h, and cooling to the operating temperature. Residual hydrogen was removed by flushing with N_2 (25 mL/min, STP) for 20 min.

Evaluation of catalytic activity was performed at 498 K and 29.7 bar. The flow rates ranged from 0.1 to 1.0 mL/min; which corresponds to the weight hourly space velocities (WHSV) of 1.2−9.6 h^{-1} calculated as mass of the substrate per mass of the catalyst per hour ($g_{subst}\cdot g_{cat}^{-1}\cdot h^{-1}$). The same flow rate was kept for at least 4 h in order to reach the steady state. Deactivation of the commercial 2.5 wt % Pt/C catalyst was tested by repeating the same flow rate (0.2 mL/min) 4 times in between the others.

Additional studies of methanation and water gas shift (WGS) were performed on the Pt−Re/C catalyst (0.5 g) at 498 K and 25 bar. Liquid water (0.2 mL/min, HPLC pump) was fed together with CO (8 mL/min, STP), hydrogen (8 mL/min, STP), and nitrogen (8 mL/min, STP) in the methanation experiment, which lasted for 15 h. Thereafter, the hydrogen flow was stopped, and CO flow was increased to 16 mL/min (STP) for the next 6 h during the WGS experiment.

Gas products were quantitatively analyzed online by a micro-GC (Agilent Micro-GC 3000A) equipped with four columns: Plot U, OV-1, Alumina, and Molsieve.

Analysis of the liquid products was performed by HPLC (Agilent 1100) equipped with an Aminex HPX-87H column. The analysis was performed at 45 °C under isocratic conditions and flow rate 0.6 mL/min. The mobile phase consisted of 5 mM H_2SO_4 water solution. The products were analyzed by using a refractive index detector (RI).

The total carbon balance was 85−100%.

The following equations were used to quantify the results of experiments.

Conversion of the substrates:

$$\text{Conversion}\ (\%) = \frac{\nu(C_{\text{xyl in}}) - \nu(C_{\text{xyl out}})}{\nu(C_{\text{xyl in}})}\cdot 100\% \quad (1)$$

where $\upsilon(C_{\text{xyl in}})$ is molar flow of carbon in the input xylitol [mol/min] and $\upsilon(C_{\text{xyl out}})$ is molar flow of carbon in the output xylitol [mol/min].

For alkanes, CO_2, CO, and products in the liquid phase, selectivity was calculated in the following way:

$$\text{Selectivity to product X}\ (\%) = \frac{\upsilon(C_X)}{\upsilon(C_{\text{gas}})}\cdot 100\% \quad (2)$$

where $\upsilon(C_x)$ is molar flow of carbon, contained in a product [mol/min], $\upsilon(C_{\text{gas}})$ is molar flow of carbon, contained in all gas-phase products, such as CO_2, CO and alkanes [mol/min].

An additional parameter, namely, the so-called reforming ratio RR (H_2/CO_2), was introduced to calculate the selectivity to hydrogen, because hydrogen is produced both from xylitol and via the water gas shift reaction:

$$C_5H_{12}O_5 \rightarrow 5CO + 6H_2 \xrightarrow{+6H_2O} 5CO_2 + 11H_2$$

Selectivity to hydrogen is defined in the following way:

$$\text{Selectivity to}\ H_2\ (\%) = \frac{\upsilon(C_{H_2})}{\upsilon(C_{\text{gas}})}\cdot\frac{1}{\text{RR}}\cdot 100\% \quad (3)$$

where $\upsilon(H_2)$ is moles of H_2 formed and RR = 11/5 for xylitol.

The molar flow of carbon $\nu(C_X)$ is determined as

$$\nu(C_X) = C_X\cdot\upsilon\cdot n \quad (4)$$

where C_X is the molar flow of a substance X [mol/L·min], υ the volumetric flow [L/min], and n the number of carbon atoms in the substance.

Turnover frequency for xylitol transformation [TOF(xyl)] and H_2 production [TOF(H_2)] was defined per mole of surface metal atom. In the case of bimetallic catalysts, only Pt loading was taken into account. TOF_{xyl} is calculated as

$$\text{TOF(xyl)} = \frac{\nu_{\text{xyl in}} - \nu_{\text{xyl out}}}{D\cdot m_{\text{cat}}\cdot c_M\cdot M_M} \quad (5)$$

where $\upsilon_{\text{xyl in}}$ is the input molar flow of xylitol [mol/min], $\upsilon_{\text{xyl out}}$ the output molar flow of xylitol [mol/min], D the metal dispersion, m_{cat} the catalyst loading [g], c_M the metal loading, and M_M the molar mass of metal.

Turnover frequency for H_2 is determined as

$$\text{TOF}(H_2) = \frac{\nu_{H_2}}{D\cdot m_{\text{cat}}\cdot c_M\cdot M_M} \quad (6)$$

where υ_{H_2} is hydrogen molar flow [mol/min].

3. RESULTS AND DISCUSSION

The characterization data for all studied catalysts except 2.5 wt % Pt/C provided by Johnson Matthey are given below. The Pt/C catalyst is also described elsewhere.[73]

3.1. Nitrogen Physisorption on Sibunit. The support has a surface area of 247 m^2/g. The external surface area is 60 m^2/g, and the total pore volume is 0.24 cm^3/g. The support has a mesopourous structure with a small volume of micropores. According to the IUPAC classification, nitrogen adsorption isotherms at 77 K correspond to Type I with capillary condensation hysteresis loop of H3 type. This indicates the presence of both micro- and mesopores. The mesopores are most probably formed between planes of flat or polyhedral primary carbon particles. The material has no pores with the size exceeding 5 nm in the studied 2−100 nm range.

The surface area of catalysts should be negligibly affected by metal impregnation. Comparison of surface areas of fresh and spent catalysts was not possible because the latter cannot be separated from the sand used in the catalyst testing. Analysis of the mixed phase is hindered probably because of uneven mixing of catalyst with the quartz sand.

3.2. TEM. The detailed description of the particle size distribution is given in Table 3. Transmission electron microscopy images of fresh and used carbon-supported

DOI: 10.1021/acs.iecr.7b04937
Ind. Eng. Chem. Res. 2018, 57, 2050−2067

Table 3. Results of TEM Measurements of Carbon-Supported Catalysts

catalyst	Dn[a] [nm]	Ds[b] [nm]	SD [nm]	dispersion[c] [%]
		fresh/**spent**		
2.5% Pt/C	2.05/**1.7**	2.05/**1.8**	0.55/**0.3**	20.1
3% Pt/C	0.9/**1.2**	1/**1.2**	0.2/**0.2**	45.8
Ni/C	7.7/**n.a.**	8.6/**n.a.**	1.9/**n.a.**	13.1
Pt−Ni/C	Pt 1.2/**1.2**, Ni 8.5/**n.a.**		Pt 0.2/**0.2**, Ni 1.4/**n.a.**	Pt 34.4, Ni 11.9
Re/C	<0.5/**0.7**	<0.5/**0.7**	0.1/**0.1**	82.5
Pt−Re/C	1.1/**n.a.**	1.1/**n.a.**	0.2/**n.a.**	37.5
Ru/C	1/**1.2**	1.1/**1.3**	0.1/**0.2**	41.2
Pt−Ru/C	1.3/**1.4**	1.6/**1.5**	0.4/**0.3**	31.7
Pt−Co/C	1.3/**1.3**	1.5/**1.4**	0.3/**0.2**	31.7

[a]Ds is surface average diameter, $Ds = \frac{\Sigma n_i \cdot d_i^3}{\Sigma n_i \cdot d_i^2}$, where n is number of particles and d is particle diameter. [b]Dn is number-average diameter, $Dn = \frac{\Sigma n_i \cdot d_i}{\Sigma n_i}$. [c]Dispersion of metals was calculated based on metal particle diameters obtained from TEM measurements for the fresh catalysts.

catalysts are shown in the Supporting Information (Figures S1 and S2). All catalysts have well-dispersed metal particles with some areas of agglomerations. The medium particle size is about 1 nm, except for Ni catalyst that showed a mean value of 7.7 nm. Pt−Ni catalyst showed a distinct bimodal distribution with noticeably smaller Pt and bigger Ni species. Data in both Figure 2 and Table 3 confirm that there was essentially no sintering under conditions of the xylitol APR.

Calculation of the metal dispersion for fresh catalysts was based on TEM measurements. Metal particles were assumed to be truncated octahedrons except for Ni clusters, which could be described by a spherical shape model being larger than 1.2 nm.[75] The strength of metal−support interaction influences the ratio between the surface and the total amount of metal atoms.[76] Interactions between particles and a support were claimed to be weaker for carbon supports than for metal oxides.[77] Thus, the dispersion for the truncated octahedrons was calculated as the total surface with a subtracted area of one hexagonal face divided by the total volume:

$$D = \frac{(6 + 12\sqrt{3})\cdot a^2 - 2\sqrt{3}\cdot a^2}{8\sqrt{2}\cdot a^3} = \frac{3 + 5\cdot 3}{2\sqrt{2}\cdot d} \quad (7)$$

where a is the facet length and d is the particle diameter.

The dispersion for spherical Ni particles was calculated in the following way:

$$D = \frac{6\cdot V_M}{A_M \cdot d} \quad (8)$$

where the atomic volume V_M is 10.95 Å^3 and the area occupied by a surface nickel atom A_M is 6.51 Å^2.

Metals in all catalysts are well-dispersed except for Ni/C and Ni particles in Pt−Ni/C. The highest dispersion was displayed for Re/C catalyst, being as high as 82.5%.

3.3. TG-DTA-MS. The results of thermogravimetric studies curves are shown in Figure 2. Pt, Ru, Pt−Ru, and Pt−Co were reduced in 15% H_2/Ar, and the peaks corresponding to mass losses are attributed to reduction of the metal. Catalysts on the basis of nitrate precursors such as Ni, Pt−Ni, as well as Re and Pt−Re were heated at 573 K in argon to decompose nitrates and then reduced in 15% H_2/Ar. The minor mass losses occurred in all catalysts at temperatures below 493 K, which can be attributed to reduction of MeO_x. For some samples, neither water nor chlorides can be attributed to mass losses according to MS data.

3.4. EDX. Energy-dispersive X-ray spectroscopy was used to analyze Pt and Ni catalysts. The images can be found in Figure S3. No major impurities were found. Minor side signals appeared from the copper grid.

3.5. XPS. X-ray photoelectron spectroscopy was used to analyze Pt, Ni, Pt−Ni, and Re catalysts in order to identify the electronic state of metals presented mainly on the surface of tested materials. Catalysts were reduced at temperatures mentioned in Table 2 prior to the analysis. XPS deconvolved spectra are presented in Figures 3 and 4. According to the XPS data, all reduced catalysts contained metal in mixed oxidation states. The Pt 4f binding energy of 71.3 eV was assigned to zerovalent Pt. No significant shifts were observed for binding energies of Pt^0 or Pt^{x+} after addition of a second metal, such as Ni or Co. However, a 0.2 eV shift to higher binding energy value was found in Pt−Ru for Pt^{4+}, which can be attributed to a strong interaction between Pt and Ru. The reduction degree of

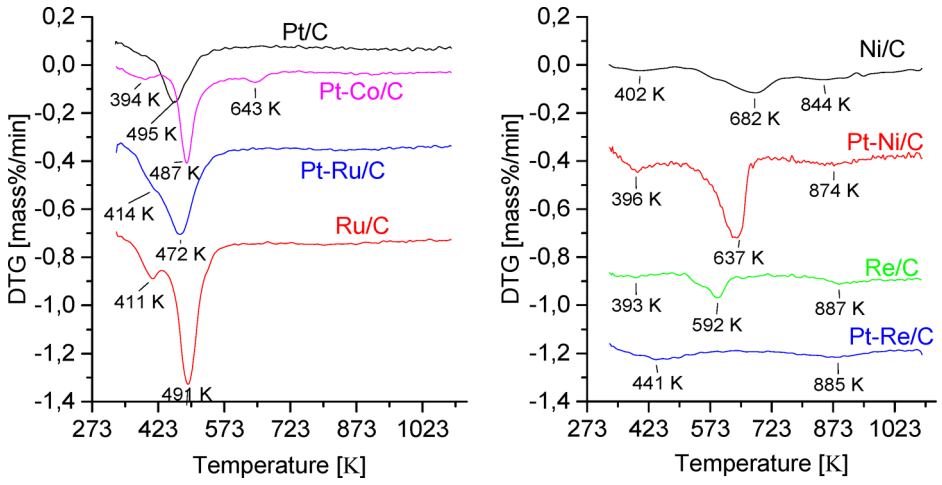

Figure 2. Thermogravimetric studies of catalyst reduction. Catalysts on the left side were reduced in 15% H_2 (Ar). Catalysts on the right side were heated at 573 K in argon to decompose nitrates and then reduced in 15% H_2 (Ar).

DOI: 10.1021/acs.iecr.7b04937
Ind. Eng. Chem. Res. 2018, 57, 2050−2067

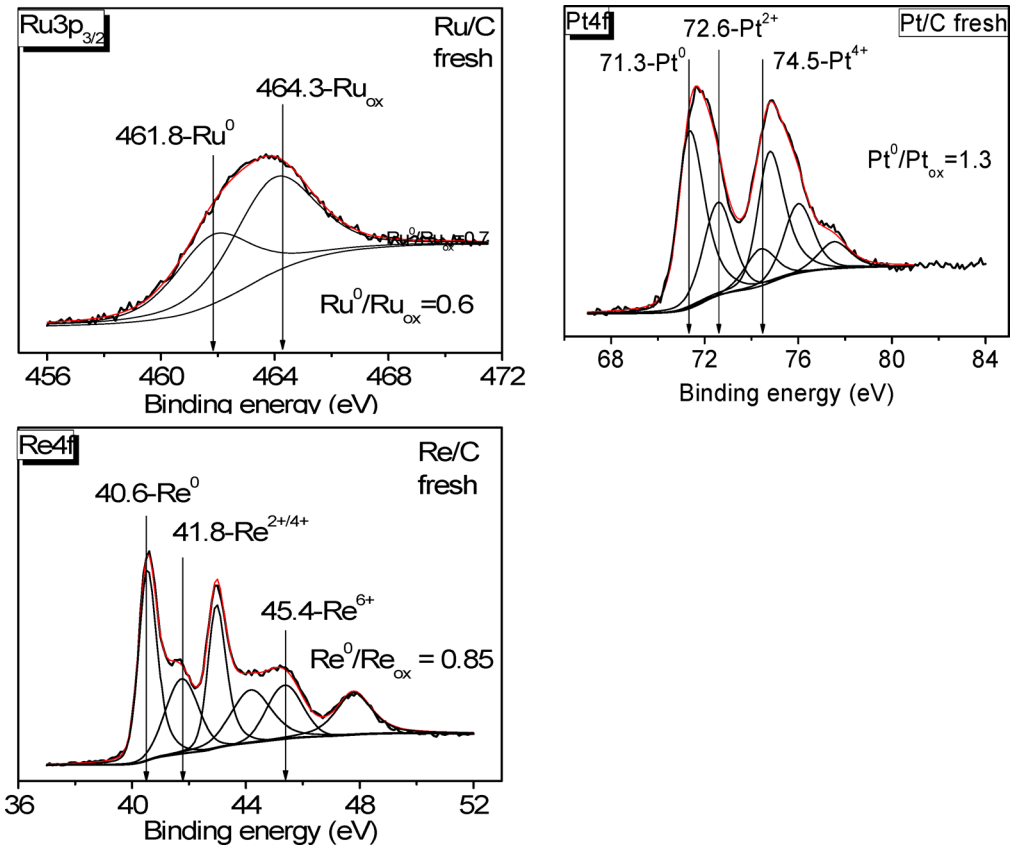

Figure 3. Deconvolved XPS spectra of fresh Pt/C, Re/C, and Ru/C catalysts.

platinum was 56.5% in Pt/C, 80.8% in Pt−Ni/C, and 59.4% in Pt−Co/C. At the same time, only oxidized species Pt^{2+} and Pt^{4+} were found in Pt−Ru/C.

The reduction degree of ruthenium was 37% in Ru/C and 46% in Pt−Ru/C. Rhenium catalyst is oxidized to a mixture of oxidation states, including 0, +2, +4, and +6, showing the reduction degree of 46%. Ni and Co were not fully reduced in both bimetallic catalysts Pt−Ni/C and Pt−Co/C.

The bimetallic catalyst Pt−Co/C has lost almost all cobalt during the APR experiment, as can be seen from the Figure 4. The signal of Ni_{2p} is similar for the fresh and used Pt−Ni/C samples, despite the green coloring of the liquid samples attributed to nickel leaching.

3.6. XRD. For the majority of the samples, it was shown that reduction at temperatures selected on the basis of preliminary TPR measurements proceeds completely. However, for several samples containing easily oxidized or highly dispersed particles where overlapping with carbon reflections also occurred, additional XRD measurements to identify the crystal phase were carried out.

According to XPS data, the Re/C sample contains Re in a high oxidation state along with metallic rhenium. XRD patterns of this sample showed presence of Re only in the reduced stated as neither Re oxides nor $HReO_4$ phase were visible. Similar Re reflections were observed for Re/C reduced at 591 and 645 K. XPS results can be rationalized by existence of well-dispersed Re in higher oxidation states which cannot be detected by XRD.

3.7. XRF. XRF was used to determine the metal content for Pt, Re, Ru, Pt−Ni, and Pt−Re catalysts. Results of XRF measurements are presented in Table 2. It can be seen from this table that the obtained values are consistent with the nominal loading. While the content was not determined for Ni/C, Pt−Ru/C, and Pt−Co/C catalysts, because of the same incipient wetness impregnation preparation method and the same metal salts solutions it can be safely assumed that the metal loading is very close to the nominal one also for those catalysts.

3.8. Ammonia Desorption. Acidity of catalysts was evaluated by ammonia desorption, which was performed in the temperature range not exceeding 498 K or the APR reaction temperature. The desorption curves are presented in Figure 5, while the desorption energies and the total number of acid sites are shown in Table 4. The desorption energy is close to 40 kJ/mol·K for all catalysts except for Ru, Pt−Ru, Pt−Co, and the commercial 2.5% Pt/C. Data is consistent with earlier reported values for Pt/C and Pt/Sibunit in the range of 45−54 kJ/mol·K.[50] An insignificant amount of ammonia was detected during desorption from the bare support Sibunit.

The amount of acid sites varies from 5 to 12 μmol NH_3/g catalyst depending on the active metal. Pt−Ni and the commercial 2.5% Pt/C catalyst had a noticeably higher number of acid sites being able to adsorb 29.3 and 21.3 μmol NH_3/g catalyst, respectively.

3.9. Catalytic Performance: Mass-Transfer Limitations. The absence of internal mass-transfer limitations was confirmed by the Weisz−Prater criterion, Φ_{WP}.

$$\Phi_{WP} = \frac{r_{w,p}^{obs} \cdot \rho_{cat} \cdot r_p^{\,2}}{D_e \cdot C_s} \tag{9}$$

,where $r_{w,p}^{obs}$ is the observed reaction rate per kilogram of catalyst [mol/s·kg cat], ρ_{cat} the catalyst density [kg/m^3], r_p the catalyst

DOI: 10.1021/acs.iecr.7b04937
Ind. Eng. Chem. Res. 2018, 57, 2050−2067

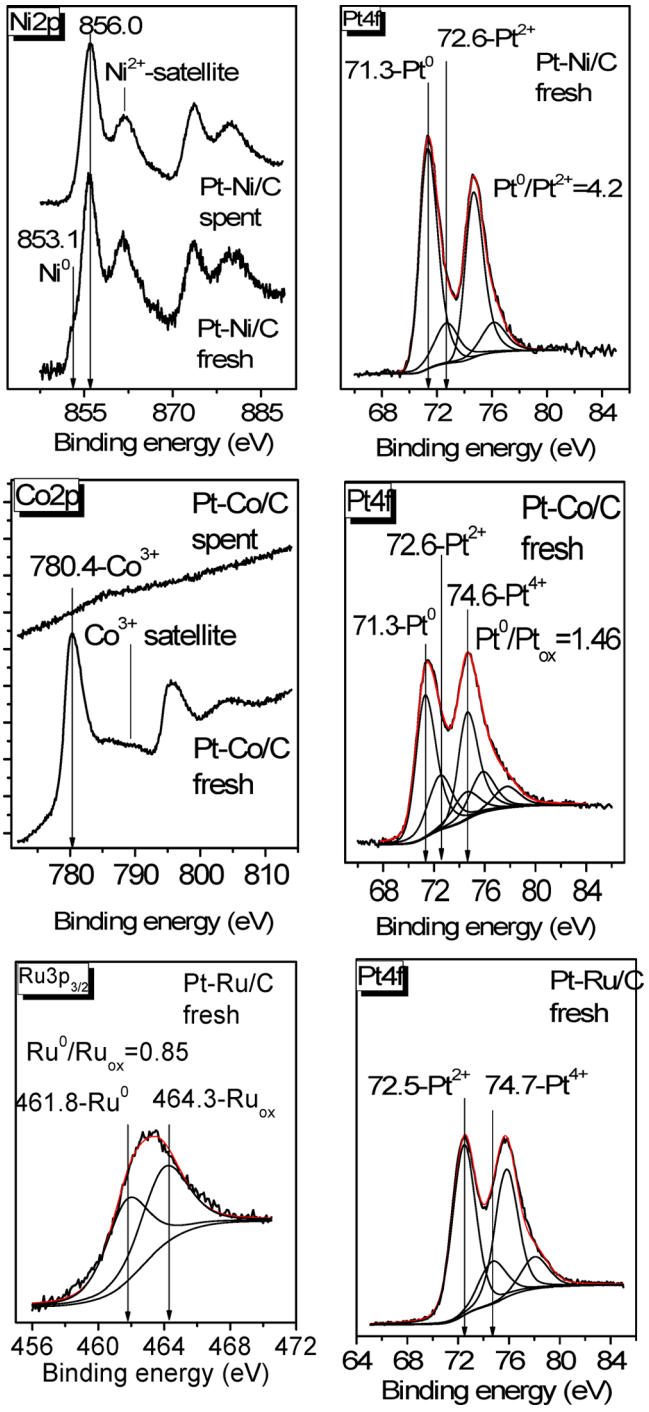

Figure 4. Deconvolved XPS spectra of fresh Pt−Ru/C and fresh and spent Pt−Ni/C and Pt−Co/C catalysts.

particle radius [m], D_e the effective diffusion coefficient [m^2/s], and C_s the surface feed concentration [mol/m^3].

The dimensionless criterion Φ_{WP} confirms a sufficient condition for the absence of significant pore diffusion limitations. For a zero-order reaction, Φ_{WP} should be lower than 6; for a first-order, lower than 0.6; and for a second-order, lower than 0.3.

The fastest reaction rate and the largest catalyst particles were taken into consideration. The reaction rate $r_{w,p}^{obs}$ observed on the Pt−Re catalyst was 1.38×10^{-2} mol/s·kg cat. The Sibunit support density varies in general from 300 to 800 kg/m^3 depending on the particle size and other parameters. Catalyst density was taken to be 650 kg/m^3. The largest catalyst particles radius r_p was 90 μm. Concentration of the feed at the catalyst surface C_s is assumed to be equal to the bulk concentration, namely 658 mol/m^3. The effective diffusion coefficient D_e is defined as

$$D_e = D \cdot \frac{\xi}{\chi} \tag{10}$$

where the ratio between porosity ξ and tortuosity χ is assumed to be 0.1.

According to *Perry's Chemical Engineers' Handbook*,[78] the Siddiqi−Lucas equation gives a lower average absolute deviation compared to the Wilke−Chang equation for calculation of the diffusion coefficient D of miscellaneous nonelectrolytes in water. The diffusion coefficient of xylitol in water according to Siddiqi and Lucas is defined as

$$D_{AW} = 2.98 \times 10^{-7} \cdot V_A^{-0.5473} \cdot \eta_W^{-1.026} \cdot T \tag{11}$$

Water dynamic viscosity η_W at the reaction conditions is estimated to be 0.1188 cP according to Reid et al.[79] Molar volume of xylitol at boiling point V_A = 155.4 cm^3/mol is calculated via the additive method proposed by Le Bas.[80]

The calculated diffusion coefficient D_{AW} is 8.34×10^{-5} cm^2/s. The effective diffusion coefficient D_e is 8.34×10^{-10} m^2/s.

The Weisz−Prater criterion confirms the absence of internal mass-transfer limitations being lower than 0.6:

$$\Phi_{WP} = \frac{1.38 \times 10^{-2} \cdot 650 \cdot (90 \times 10^{-6})^2}{8.34 \times 10^{-10} \cdot 657.89} = 0.13 \tag{12}$$

3.10. Trickle Flow Region. The flow regime in the reactor can be classified as a trickle flow according to Sie and Krishna.[81] The gas flow is 1.26×10^{-4} m/s, and the liquid flow varies from 0.0147 to 0.147 kg/m^2·s, or from 1.77×10^{-5} to 1.77×10^{-4} m/s. Those values are located within the trickle flow regime for the cocurrent downflow diagram obtained for an air−water system. The transition regions between trickle and pulse flows are shifted to higher flow velocities with an increased pressure according to Saroha and Nigan.[82]

3.11. Catalytic Experiments. *3.11.1. Activity.* In the current study, mono- and bimetallic catalysts were compared in terms of activity, selectivity to hydrogen, and total selectivity to alkanes. Catalyst activity was determined as conversion of the initial feed. Dependence of conversion versus WSHV for all studied catalysts is shown in Figure 6. TOF values based on xylitol conversion for three different WSHV values are presented in Figure 7.

The commercial catalyst 2.5 wt % Pt/C supported on powder activated carbon is slightly more active compared to 3 wt % Pt/C supported on granular activated carbon Sibunit. TOF of the commercial catalyst is above 114 min^{-1}, while TOF of the Sibunit-supported Pt was less than 20 min^{-1}. Because absence of external mass-transfer limitations was confirmed for both catalysts, differences in TOF can be explained by the difference in the metal particle sizes (0.9 nm in 3% Pt/C versus 2.05 nm in 2.5% Pt/C), a 2-fold greater amount of acid sites in the commercial catalyst.

According to Barbelli et al.[83] and Kirilin et al.,[50] catalyst activity and hydrogen turnover frequency are increasing along with the metal particle size increase. It should be noted that contradictory results regarding structure sensitivity of APR were reported in the literature. Lehnert et al.[84] concluded that

DOI: 10.1021/acs.iecr.7b04937
Ind. Eng. Chem. Res. 2018, 57, 2050−2067

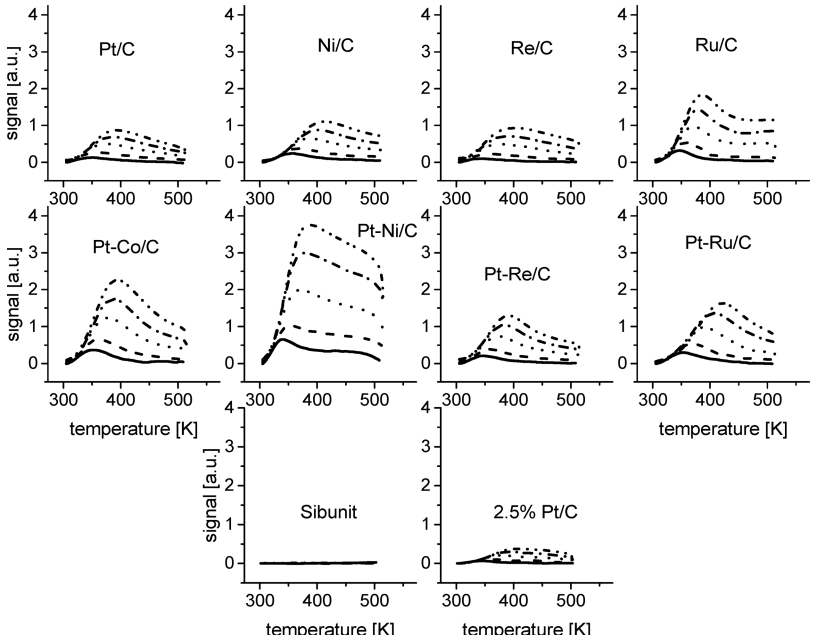

Figure 5. Ammonia desorption curves for Sibunit-based catalysts, the commercial 2.5% Pt/C, and the Sibunit support with the following heating rates: solid line, 3 K/min; dashed line, 5 K/min; dotted line, 10 K/min; dash−dotted line, 15 K/min; dash−double dotted line, 20 K/min.

Table 4. Results of Acidity Measurements of Carbon-Supported Catalysts and the Sibunit Support

catalyst	E_{des} [kJ/mol·K]	acidity [μmol NH_3/g catalyst]
Sibunit	0	0
2.5% Pt/C	32.0	21.9
3% Pt/C	40.8	5.2
Ni/C	38.0	7.5
Pt−Ni/C	39.0	29.3
Re/C	30.0	5.9
Pt−Re/C	42.8	6.7
Ru/C	50.7	11.7
Pt−Ru/C	28.0	7.9
Pt−Co/C	46.3	12.5

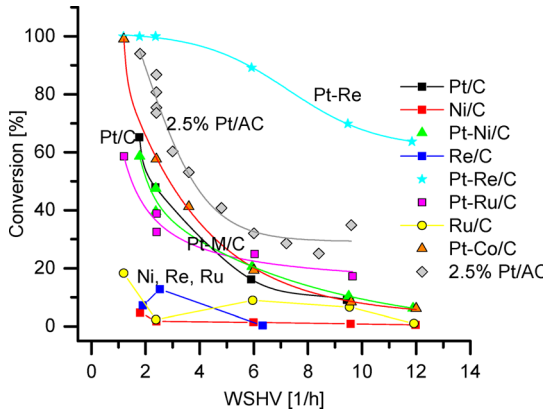

Figure 6. Conversion of xylitol in APR on carbon-supported catalysts as a function of WHSV. The following conditions were used: xylitol concentration was 100 g/L; T = 498 K; P = 29.7 bar; mass of catalyst was 0.5 g.

the reaction rate is not affected by changes in the particle size: Pt catalysts with sizes ranging from 1.6 to 3.1 nm showed similar activity in the glycerol APR. According to Chen et al.,[85] total carbon conversion from the liquid to the gas phase even decreased along with the Pt particle increase in the APR of bio-oil low-boiling fraction over Pt/Al_2O_3.

All monometallic catalysts except Pt/C displayed significantly lower activity (e.g., Ni/C) or deactivated very fast (e.g., Ru/C, Re/C). The Re/C was completely deactivated after 30 h of time-on-stream. The activity of Ru/C significantly decreased after 50 h of time-on-stream. Poor performance of Re/C[27,44] catalysts was already discussed in the literature. However, Ru/C catalyst was as active as Pt/C in the APR of sorbitol in a fixed-bed reactor[51] and in the APR of wheat straw hydrolysate in a batch reactor.[34] Ru/CNF catalyst was also active and stable in the APR of acetic acid.[59]

The performance of nickel-containing catalysts was probably affected by Ni leaching. All liquid-phase samples collected during the experiments with Ni and Pt−Ni catalysts (54 and 74 h TOS, respectively) had a slightly green color, which can be presumably explained by formation of Ni complexes with reaction intermediates. It was reported that CNF-supported Ni catalyst is prone to leaching in the sorbitol or ethylene glycol APR, unless an initial hydrogen atmosphere was applied or a base additive was introduced.[37] In the same study it was shown that a substantial growth of Ni nanoparticles and coke formation caused a substantial loss of the metal surface area.

Activity of bimetallic Pt−Ni and Pt−Co catalysts was practically on par with the monometallic one, while Pt−Ru catalyst was slightly more active. TOF of those bimetallic catalysts varied from 16 to 33 min^{-1}, while the Pt catalyst showed slightly lower values. Thus, it can be assumed that addition of the second metal enhanced the activity of Pt. An outstanding high activity was displayed by Pt−Re catalyst. TOF of this catalyst is decreasing with a flow rate increase because conversion reached 100% already at the WSHV interval from 2.4 to 6 h^{-1}. The highest amount of xylitol per mole of surface Pt was converted over Pt−Re/C.

Activity distribution obtained in the current study correlates with the results published previously by Kunkes et al.[21] for glycerol APR over bimetallic catalysts supported on carbon black. The fact that Pt−Re catalysts are much more active than

DOI: 10.1021/acs.iecr.7b04937
Ind. Eng. Chem. Res. 2018, 57, 2050−2067

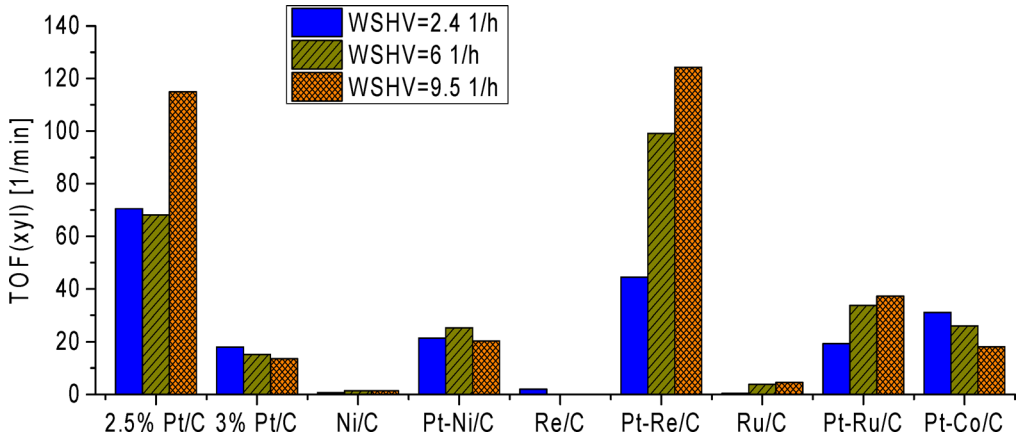

Figure 7. TOF_{xyl} (min^{-1}) of carbon-supported catalysts in xylitol APR at different WHSV and xylitol concentration 100 g/L, T = 498 K, P = 29.7 bar, and mass of catalyst 0.5 g.

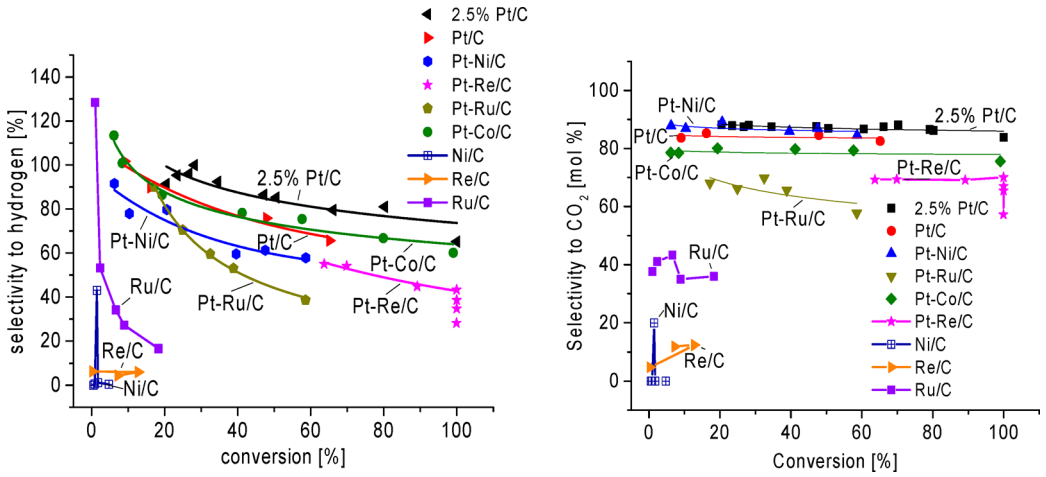

Figure 8. Selectivity to H_2 (left) and CO_2 (right) for APR of xylitol over carbon-supported catalysts as a function of conversion. The following conditions were used: xylitol concentration was 100 g/L; T = 498 K; P = 29.7 bar; mass of catalyst was 0.5 g.

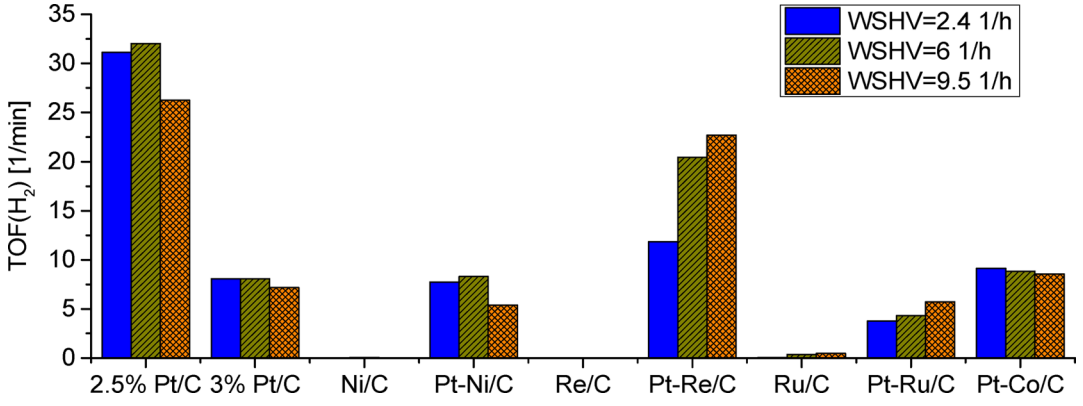

Figure 9. Hydrogen TOF (min^{-1}) of carbon-supported catalysts in xylitol APR at different WHSV. The following conditions were used: xylitol concentration was 100 g/L; T = 498 K; P = 29.7 bar; mass of catalyst was 0.5 g.

monometallic Pt counterparts was already shown for APR of glycerol[27,46,54,55] and transformations of glycerol in the gas phase on carbon-supported Pt−Re catalysts.[86] Moreover, it was demonstrated that addition of Re increases the rates of WGS reaction and alkane formation.[46]

As discussed in the Introduction, APR reaction needs to be considered sensitive to process conditions, which influence the product distribution and conversion. Thus, the catalytic activity obtained in the current study can be compared directly with the results published in the literature only if the following requirements are met: the same feed, substrate concentration, temperature, reactor type, and catalyst amount are applied. Moreover, preferably experiments are conducted under similar carrier-gas flows and pressure and with similar metal loading.

Just two publications fall into this category. Namely, Kirilin et al.[50] studied the APR of xylitol over 2.8% Pt/CDC. The

DOI: 10.1021/acs.iecr.7b04937
Ind. Eng. Chem. Res. 2018, 57, 2050−2067

observed conversion was 12% at WSHV = 3 h^{-1}, while in the current study much higher values were obtained: 48% at WSHV = 2.4 h^{-1} over 3% Pt/C and 51% at WSHV = 3 h^{-1} over the commercial 2.5% Pt/C. Similar catalytic activity were observed by Kirilin et al.[50] for commercial 5% Pt/Al_2O_3. Duarte et al.[9] reported conversion of 4.2% at WSHV = 12 h^{-1} in the APR of xylitol over 2.77% Pt/Al_2O_3, while in the current study Pt−Ni/C and Pt−Co/C both exhibited 6% conversion at the same WSHV.

3.11.2. Selectivity. Selectivity to hydrogen is decreasing along with conversion increase for all catalysts (Figure 8), as it can be expected for consecutive reactions. The highest selectivity was obtained with the commercial 2.5 wt % Pt/C. Sibunit-supported Pt/C and Pt−Co/C exhibited very similar performance. The same holds for slightly less selective Pt−Ni and Pt−Re. It is interesting that all Pt mono- and bimetallic catalysts displayed hydrogen selectivity curves that are parallel to each other, in contrast to Pt−Ru. Monometallic Ni, Re, and Ru turned out to be the worst candidates for hydrogen production.

TOF(H_2) is presented in Figure 9. The commercial Pt catalyst generated the largest amount of hydrogen per mole of surface Pt. It is visible from Figure 9 that TOF values did not change much along with WHSV and thus conversion in the case of all catalysts except Pt−Re/C and Pt−Ru/C. This can be explained by deviations from the zero-order kinetics in the latter cases.

Current results can be compared to the literature taking into account several restrictions mentioned above in the subsection related to conversion part. Selectivity to hydrogen was 77% (obtained at 56% xylitol conversion) in the APR of xylitol over 2.8% Pt/CDC[50] and is comparable to the value of 83% (at 60% xylitol conversion) for the commercial 2.5% Pt/C reported in this study. At the same time, the alumina-based catalyst used by Duarte et al.[9] showed 98% selectivity to hydrogen at 4% conversion of xylitol, while in the current study only 85% selectivity was obtained at 5% conversion of xylitol. TOF to hydrogen obtained in the current study over both Pt catalysts exceeds substantially the values obtained by Kirilin et al.[50]

The overall trends for selectivity to CO_2 are similar to those for hydrogen. Commercial 2.5% Pt/C, Pt/C, Pt−Ni/C, and Pt−Co/C are more selective to CO_2 (80−90% selectivity) compared to Pt−Ru and Pt−Re, which showed 60−70% selectivity. Moderate values (around 40%) were obtained on Ru, while Re and Ni exhibited a very low performance.

Total selectivity to alkanes (Figure 10) was calculated as a sum of selectivity to all determined hydrocarbons: methane, ethane, propane, *n*-butane, *n*-pentane, *iso*-pentane, *neo*-pentane, *n*-hexane, *iso*-hexane, and *n*-heptane. Formation of C_6−C_7 alkanes can be explained by condensation reactions.[87] Neither *iso*-butane nor unsaturated compounds were found among the gas products. Ru-, Ni-, and Re-based catalysts exhibited the highest overall selectivity to alkanes among all catalysts. Pt/C, 2.5% Pt/C, and Pt−Ni/C bimetallic catalysts appeared to be practically identically selective to alkanes (11−17%). Addition of Co to Pt increased selectivity to alkanes almost 2-fold (20−25%). Pt−Ru is apparently more selective to alkanes than Pt−Re, and both of them are approximately three times more selective than Pt. A more illustrative comparison of selectivity to hydrogen is given in Figure 9 for catalysts with the best performance at 60% conversion.

A more illustrative comparison of selectivity to hydrogen and total selectivity to alkanes is given in Figure 11. The catalysts

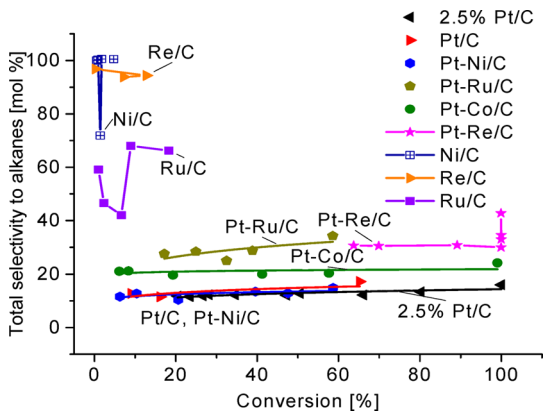

Figure 10. Overall selectivity to alkanes for studied catalysts at different conversion levels. The following conditions were used: xylitol concentration was 100 g/L; T = 498 K; P = 29.7 bar; mass of catalyst was 0.5 g.

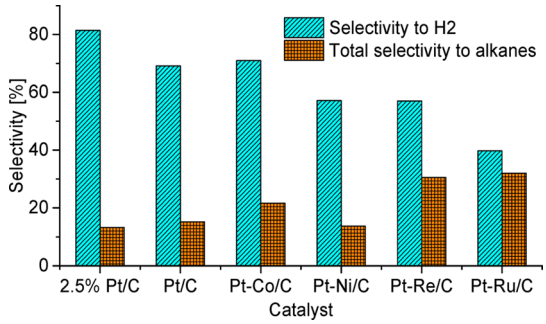

Figure 11. Selectivity to H_2 for APR of xylitol over selected carbon-supported catalysts for comparable conversion range 58−66%. The following conditions were used: xylitol concentration was 100 g/L; T = 498 K; P = 29.7 bar; mass of catalyst was 0.5 g.

with the best performance are compared 58.5% conversion. The selectivity was taken from the data fitted via an allometric power function. Commercial 2.5% Pt−C catalyst exhibited the highest selectivity to hydrogen and lowest selectivity to alkanes. Among Sibunit-supported catalysts, Pt/C and Pt−Co/C are more selective to hydrogen compared to the others. However, Pt−Co/C shows 20% selectivity to alkanes, while Pt/C shows a lesser value of 17%. Pt−Ni/C and Pt−Re/C exhibited similar selectivity to hydrogen (57%); at the same time, Pt−Re/C and Pt−Ru/C appeared to be the most selective to alkanes catalysts.

A more detailed speciation of alkanes is provided in Figure 12, showing that although the overall selectivity slightly varied with conversion, selectivity to a particular alkane displayed much larger variations. Heptane is not presented in Figure 12 because of the low observed amount of C_7H_{16} (selectivity did not exceed 0.36%). Pt is active in the reactions of C−C bonds cleavage, being selective mostly to propane (ca. 5 mol %). Addition of Ni made a shift to short-chained alkanes, but it can be done even more via addition of Ru. Addition of Co increased the selectivity to methane (ca. 5 mol %, compared to 0−2.5 mol % for Pt) but also increased the selectivity to propane (7.5−10 mol %) and pentane (3−5 mol %). Pt−Re is not so active in C−C bond cleavage compared to Pt, promoting formation of butane and pentane (each with 8−10 mol % selectivity). Properties of a monometallic Ru catalyst changed dramatically during the experiment without a clear trend in selectivity. An interesting fact is that for Ni/C no alkanes with

DOI: 10.1021/acs.iecr.7b04937
Ind. Eng. Chem. Res. 2018, 57, 2050−2067

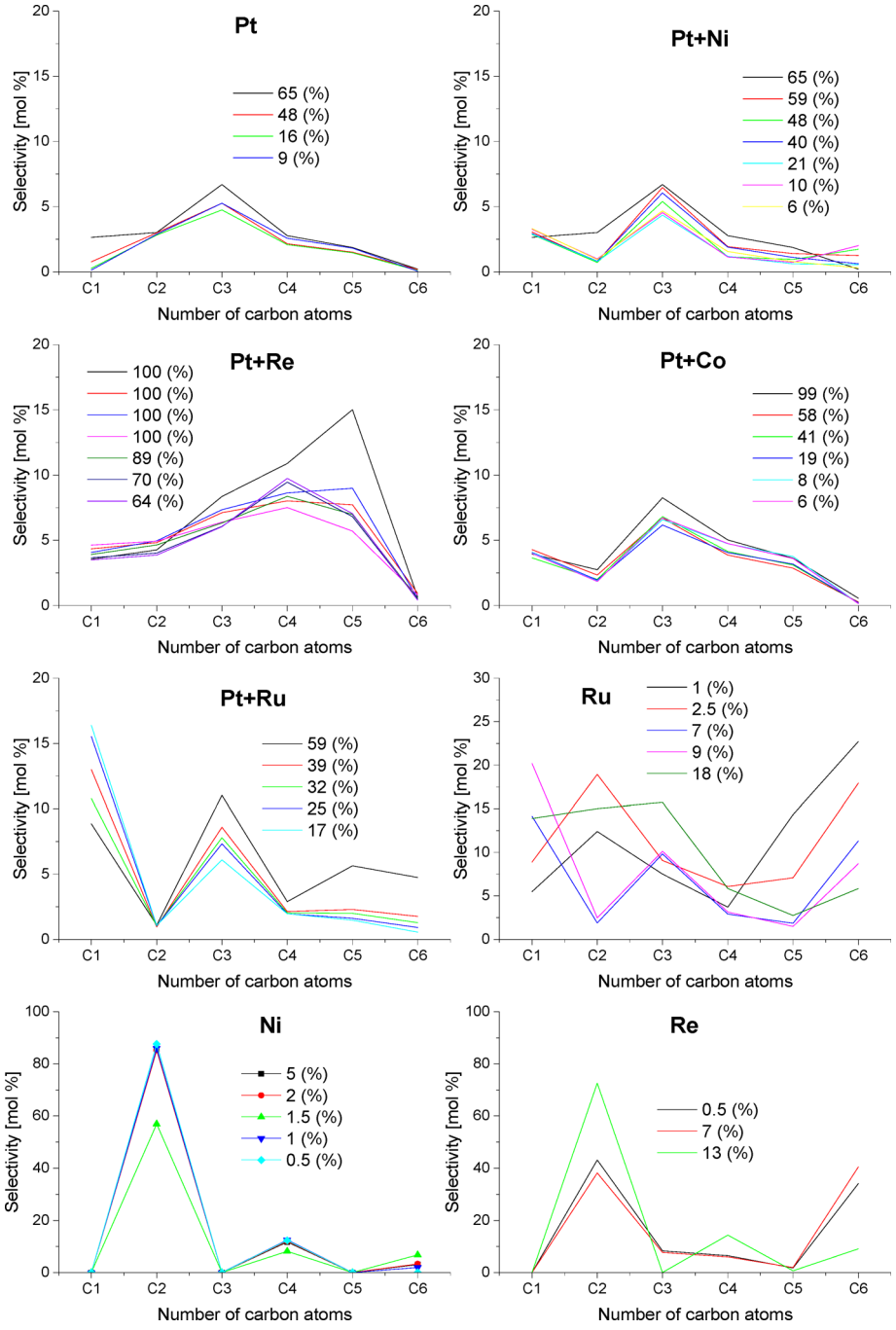

Figure 12. Selectivity to alkanes versus chain length (from C1 to C6) at different conversion levels for APR of xylitol over carbon-supported catalysts. The numbers indicate conversion level in percent. The following conditions were used: xylitol concentration was 100 g/L; T = 498 K; P = 29.7 bar; mass of catalyst was 0.5 g.

odd numbers of C atoms were found. Very similar results were obtained for Re. Ni also showed an extremely high selectivity to ethane up to 85 mol %, which is most probably related to the absence of CO_2 formation.

Huber et al.[88] reported that alkane distribution can be significantly altered by variation of the reaction media pH or the amount of solid acid mixed with the catalyst in APR of sorbitol. However, in the current study the initial conditions were identical for all catalysts. Moreover, catalysts exhibited similar low acidity, measured by ammonia thermal desorption (Table 4). The results are therefore connected exclusively with the properties of the metals.

Some of mono- and bimetallic catalysts, namely Pt−Ni, Pt−Ru, Ru, Ni, and Re, displayed a relatively high selectivity to hexane, which has not been reported previously for carbon-supported catalysts. Low activity of monometallic Ru, Ni, and Re catalysts corresponded to a low CO_2 production. This led to a high selectivity to alkanes, which can be presumably produced by hydrogenation of products obtained in condensation reactions.

Distribution of selectivity to alkanes with a different chain length for active carbon supported platinum catalyst (2.5 wt % Pt/C) is shown separately in Figure 13. The catalyst displays very similar selectivity to each alkane in the whole region of

DOI: 10.1021/acs.iecr.7b04937
Ind. Eng. Chem. Res. 2018, 57, 2050−2067

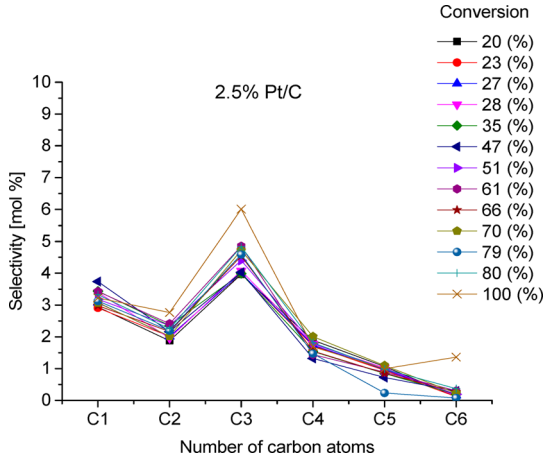

Figure 13. Selectivity to alkanes with the chain length from C1 to C6 in the xylitol APR over commercial 2.5% Pt/C catalyst at different conversion levels. The following conditions were used: xylitol concentration was 100 g/L; T = 498 K; P = 29.7 bar; mass of catalyst was 0.5 g.

xylitol conversion from 20 to 100%. Figures 12 and 13 clearly illustrate that the alkane selectivity pattern is catalyst-specific. This implies that such patterns are important characteristics of a certain metal, reflecting the ratio of various rates in the reaction network.

3.11.3. Stability. The deactivation profile of the commercial catalyst 2.5 wt % Pt/C has been presented elsewhere.[73] The catalyst showed a minor decrease of conversion and even less pronounced increase of selectivity to H_2 and CO_2 with TOS. Those changes did not influence the selectivity to individual alkanes, as can be seen from Figure 16.

On the contrary, the behavior of Ni/C catalyst changed dramatically during the very first hours of the experiment. Only the first sample after 4 h time-on-stream showed a reasonable 43% selectivity to hydrogen. For all other samples taken after 20 h time-on-stream the concentration of hydrogen in the gas phase was two orders lower, decreasing hydrogen selectivity to zero. Simultaneously, 85% selectivity to ethane was observed (with 100% total selectivity to alkanes), indicating that all hydrogen generated by APR was immediately consumed in hydrogenation/hydrogenolysis reactions. A similar behavior was observed for Re/C: deactivation took place simultaneously with fast hydrogenation decreasing selectivity to hydrogen to 4−6% and elevating selectivity to alkanes to 95%. Monometallic Ru also showed a similar behavior, although formation of alkanes was not that prominent.

3.11.4. Liquid-Phase Intermediates. Liquid-phase samples were analyzed by HPLC. Six samples were chosen for comparison between mono- and bimetallic catalysts containing Pt, as qualitatively illustrated by Figure 14 featuring corresponding chromatograms. Conversion of xylitol was close to 60% in all of them. A general view of chromatograms is given at the bottom of the graph. The upper zoomed fragment of the graph shows two major peaks of xylitol (11.2 min) and meso-erythritol (11.8 min). The minor peaks of other products are visible in the second fragment in the middle, being rather similar for all samples excluding Pt−Re and Pt−Ru. Pt−Re catalyst showed an outstanding amount of C_4−C_5 alkanes among gaseous products, but at the same time a very low amount of erythritol was obtained. This implies that this catalyst provides less C−C scission compared to C−O scission. The distribution of alkanes for Pt−Ru at the same time cannot be easily connected with the produced amount of erythritol.

Carbon distribution between gas and liquid phases obtained over 3% Pt/C and Pt−Re/C catalysts is presented in Figure 15a. The lower part of the diagram represents the part of carbon stored in the initial feed; the middle part reflects the liquid-phase intermediates, while the upper part corresponds to carbon in the gas-phase products. In addition, total carbon balance is represented by the upper line. It can be seen from this graph that the proportion of the liquid-phase intermediates is higher for Pt−Re/C catalyst compared to Pt/C at the same xylitol conversion. This portion of carbon can be interpreted as the amount of species formed from xylitol during subsequent reactions and not transformed yet to the final products: alkanes or CO_2/CO.

Platinum and bimetallic catalysts are compared in Figure 15b. The amount of carbon in the intermediates is presented versus xylitol conversion. It is rather interesting that although APR

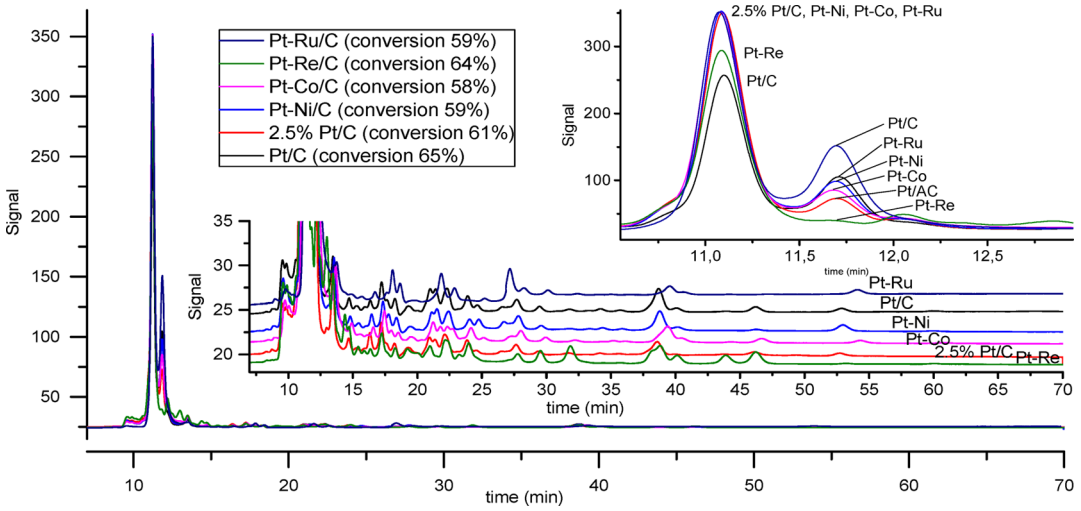

Figure 14. HPLC chromatograms of liquid-phase samples during APR of xylitol over commercial 2.5 wt % Pt/C and Sibunit-supported Pt/C, Pt−Ni/C, Pt−Co/C, Pt−Ru/C, and Pt−Re/C catalysts. The following conditions were used: xylitol concentration was 100 g/L; T = 498 K; P = 29.7 bar; mass of catalyst was 0.5 g.

DOI: 10.1021/acs.iecr.7b04937
Ind. Eng. Chem. Res. 2018, 57, 2050−2067

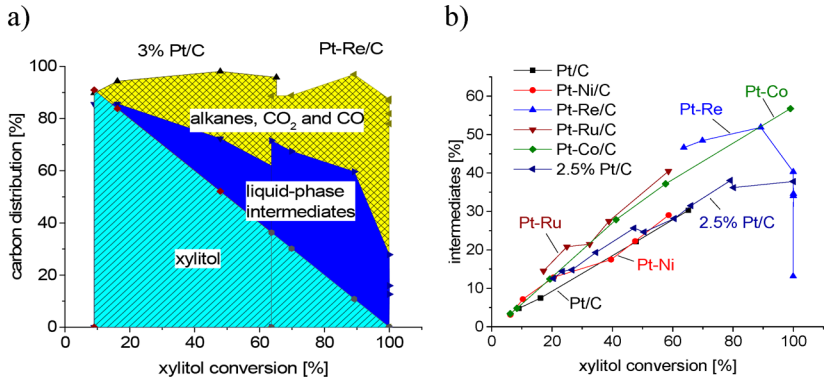

Figure 15. Carbon stored in the liquid-phase intermediates versus conversion of xylitol (a) carbon distribution among liquid and gas phases for 3% Pt/C and Pt−Re/C catalysts, (b) molar percent of carbon in the liquid-phase products in the experiments over 3% Pt/C, Pt−Re/C, PtRu/C, Pt−Ni/C, Pt−Co/C, and commercial 2.5% Pt/C. Carbon in intermediates = 100 − C_{xyl} − C_{gas}, where C_{xyl} is carbon molar flow in the unreacted feed and C_{gas} is total carbon molar flow in all gas-phase products, such as CO, CO_2, and alkanes. The following conditions were used: xylitol concentration was 100 g/L; T = 498 K; P = 29.7 bar; mass of catalyst was 0.5 g.

consists of a number of reactions, all catalysts except Pt−Re show a linear relationship between those two parameters. Another interesting observation is that the amount of carbon in the intermediates correlates with the selectivity to alkanes: the more carbon stays in the liquid, the higher the selectivity to alkanes at the same xylitol conversion. A detailed analysis of the liquid-phase intermediates could be very helpful for explanation of these observations.

3.11.5. Methanation and Water Gas Shift Reaction. Methane formation could proceed by three different reaction routes: hydrogenation of a terminal C−CH_3 with a bond scission, hydrogenation of CO, or hydrogenation of methanol. It was shown by our group before that no methane is formed from propanol-1 converted over Pt/C at 498 K and 29.7 bar.[89] This implies that neither is the −CH_2−CH_3 bond exposed to C−C scission nor is methanation happening over Pt/C. Methane formation should occur through hydrogenation of a bond between a terminal methyl group and the carbon atom bonded to oxygen: −CHOH−CH_3 or to −CO−CH_3. Another possible path is APR of an intermediate methanol.

In the current study the Pt−Re/C was tested at the conditions of WGS reaction at 25 bar and 498 K. The molar flows of gases coming from the reactor are presented in Figure 16. An initial period lasted for ca. 4 h, after which a stable state was reached. CO was almost completely converted into CO_2. The amount of CO traces increased along with the increase of CO feeding flow rate. At the same time, no methane was detected, proving the absence of methanation over the Pt−Re/C catalyst.

3.11.6. Reaction Mechanism. Reaction mechanisms of APR were proposed previously.[87,90,91] A simplified scheme of xylitol APR is given in Figure 17. The main reaction pathway is shown to result in formation of hydrogen and CO by dehydrogenation (**1**) and decarbonylation (**2**). An alternative path is hydrogenolysis (**3**) of a primary hydroxyl group with dehydration. Alkanes are formed after a complete reduction, including reduction of carbonyl groups (**4**). CO is reacting with water in a water gas shift reaction (**5**) with formation of hydrogen and CO_2. Acids can be formed from aldehydes (**6**). Various condensation reactions lead to formation of cyclic compounds and C_6−C_7 alkanes (**7**).

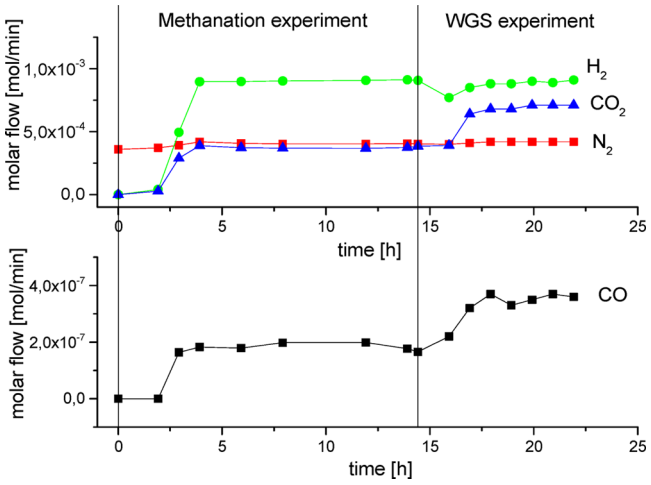

Figure 16. Methanation and WGS experiments performed over 0.5 g of Pt−Re/C catalyst at 498 K and 25 bar. Upper part: outlet molar flows of H_2, CO_2, and N_2. Lower part: outlet molar flow of CO. The input flows applied during the methanation step: water (0.2 mL/min), N_2 (1% He, 8 mL/min, STP), CO (8 mL/min, STP), H_2 (8 mL/min, STP). Hydrogen flow was stopped for the subsequent WGS step, and CO flow rate was doubled. The input flows during WGS: water (0.2 mL/min), N_2 (1%He, 8 mL/min, STP), CO (16 mL/min, STP).

4. CONCLUSIONS

Activity and selectivity of Pt, Ni, Re, Ru, Pt−Ni, Pt−Re, Pt−Ru, and Pt−Co catalysts supported on Sibunit were compared for the xylitol APR in the continuous reactor at 498 K and 29.7 bar (nitrogen) in order to determine the most appropriate metal for hydrogen production.

The Pt−Re catalyst displayed an outstanding activity compared to all other catalysts, which was accompanied by a significant selectivity to C_4−C_5 alkanes at the expense of selectivity to hydrogen. Other bimetallic catalysts showed activity levels similar to monometallic Pt. Monometallic Ni, Re, and Ru were significantly less active than Pt or bimetallic catalysts. Re and Ru were prone to deactivation already after 20 h time-on-stream. The highest selectivity to hydrogen among Sibunit-supported catalysts at xylitol conversion level of 60% was exhibited by Pt−Co catalyst. However, the same catalyst was more selective to alkanes compared to Pt.

DOI: 10.1021/acs.iecr.7b04937
Ind. Eng. Chem. Res. 2018, 57, 2050−2067

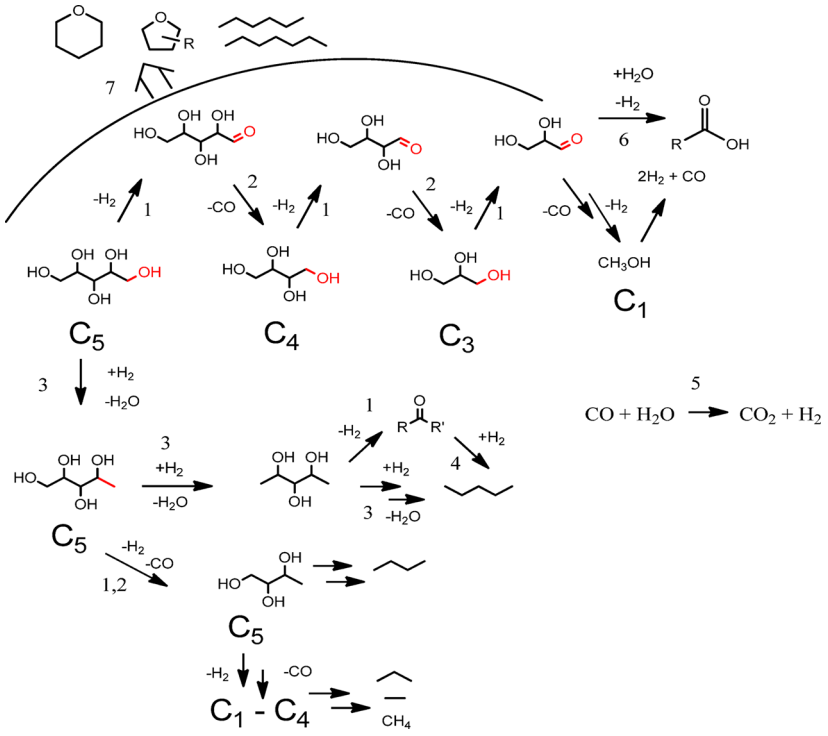

Figure 17. Simplified scheme of xylitol APR reaction mechanism.

Platinum could be the best candidate for hydrogen production from polyols via APR in terms of selectivity. However, the overall process can benefit from alkane formation by a self-sustained energy generation.[73]

While the main focus of this study was devoted to hydrogen production, an important observation was made concerning hydrocarbon production. In particular, alkane distribution was shown for the first time to be metal-specific, forming characteristic patterns not depending on the polyol conversion.

In addition, a valuable detail was added to the mechanism of methane formation. No methanation occurred at APR conditions. Methane is formed through reforming of the intermediate product, methanol, or by a bond scission between a terminal methyl group and −CHOH− or −CO− fragments via hydrogenation.

■ ASSOCIATED CONTENT

Supporting Information

The Supporting Information is available free of charge on the ACS Publications website at DOI: 10.1021/acs.iecr.7b04937.

TEM images and histograms of particle sizes of fresh and spent catalysts; EDX images of Pt/C and Ni/C catalysts (PDF)

■ AUTHOR INFORMATION

Corresponding Author

*E-mail: dmurzin@abo.fi.

ORCID

Irina L. Simakova: 0000-0002-5138-4847

Dmitry Yu. Murzin: 0000-0003-0788-2643

Present Address

§A.V.K.: Dow Benelux B.V., Herbert H. Dowweg 5, Building 443 (BBB), 4542 NM, Hoek, the Netherlands.

Notes

The authors declare no competing financial interest.

■ ACKNOWLEDGMENTS

The work was conducted within the European project SusFuelCat, which has received funding from the European Union's Seventh Framework Programme for research, technological development, and demonstration under Grant Agreement No. 310490 (www.susfuelcat.eu). A part of the work related to VIII metal group catalyst synthesis and characterization was supported by RFBR Grant 15-03-09329. The authors are grateful to Dr. Yulia Demidova from Boreskov Institute of Catalysis for valuable discussions concerning catalyst preparation and characterization. Laboratory of Wood and Paper Chemistry, Åbo Akademi University, is acknowledged for technical support.

■ REFERENCES

(1) Davda, R. R.; Shabaker, J. W.; Huber, G. W.; Cortright, R. D.; Dumesic, J. A. A Review of Catalytic Issues and Process Conditions for Renewable Hydrogen and Alkanes by Aqueous-Phase Reforming of Oxygenated Hydrocarbons over Supported Metal Catalysts. *Appl. Catal., B* **2005**, *56*, 171.

(2) Plaksin, G. V.; Baklanova, O. N.; Lavrenov, A. V.; Likholobov, V. A. Carbon Materials from the Sibunit Family and Methods for Controlling Their Properties. *Solid Fuel Chem.* **2014**, *48*, 349.

(3) Fenelonov, V. B.; Likholobov, V. A.; Derevyankin, A. Y.; Mel'gunov, M. S. Porous Carbon Materials Prepared from C1-C3 Hydrocarbons. *Catal. Today* **1998**, *42*, 341.

(4) Neira D'Angelo, M. F.; Ordomsky, V.; van der Schaaf, J.; Schouten, J. C.; Nijhuis, T. A. Aqueous Phase Reforming in a Microchannel Reactor: The Effect of Mass Transfer on Hydrogen Selectivity. *Catal. Sci. Technol.* **2013**, *3*, 2834.

(5) Neira D'Angelo, M. F.; Schouten, J. C.; van der Schaaf, J.; Nijhuis, T. A. Three-Phase Reactor Model for the Aqueous Phase Reforming of Ethylene Glycol. *Ind. Eng. Chem. Res.* **2014**, *53*, 13892.

DOI: 10.1021/acs.iecr.7b04937
Ind. Eng. Chem. Res. 2018, 57, 2050−2067

(6) Neira D'Angelo, M. F.; Ordomsky, V.; van der Schaaf, J.; Schouten, J. C.; Nijhuis, T. A. Continuous Hydrogen Stripping during Aqueous Phase Reforming of Sorbitol in a Washcoated Microchannel Reactor with a Pt−Ru Bimetallic Catalyst. *Int. J. Hydrogen Energy* **2014**, *39*, 18069.
(7) Neira D'Angelo, M. F. N.; Ordomsky, V.; Schouten, J. C.; van der Schaaf, J.; Nijhuis, T. A. Carbon-Coated Ceramic Membrane Reactor for the Production of Hydrogen by Aqueous-Phase Reforming of Sorbitol. *ChemSusChem* **2014**, *7*, 2007.
(8) Roy, B.; Sullivan, H.; Leclerc, C. A. Effect of Variable Conditions on Steam Reforming and Aqueous Phase Reforming of N-Butanol over Ni/CeO_2 and Ni/Al_2O_3 Catalysts. *J. Power Sources* **2014**, *267*, 280.
(9) Duarte, H. A.; Sad, M. E.; Apesteguía, C. R. Production of Bio-Hydrogen by Liquid Processing of Xylitol on Pt/Al_2O_3 Catalysts: Effect of the Metal Loading. *Int. J. Hydrogen Energy* **2017**, *42*, 4051.
(10) Duarte, H. A.; Sad, M. E.; Apesteguía, C. R. Bio-Hydrogen Production by APR of C2-C6 Polyols on Pt/Al_2O_3: Dependence of H_2 Productivity on Metal Content. *Catal. Today* **2017**, *296*, 59.
(11) Seretis, A.; Tsiakaras, P. Crude Bio-Glycerol Aqueous Phase Reforming and Hydrogenolysis over Commercial SiO_2 Al_2O_3 Nickel Catalyst. *Renewable Energy* **2016**, *97*, 373.
(12) Remón, J.; Giménez, J. R. R.; Valiente, A.; García, L.; Arauzo, J. Production of Gaseous and Liquid Chemicals by Aqueous Phase Reforming of Crude Glycerol: Influence of Operating Conditions on the Process. *Energy Convers. Manage.* **2016**, *110*, 90.
(13) Esteve-Adell, I.; Crapart, B.; Primo, A.; Serp, P.; Garcia, H. Aqueous Phase Reforming of Glycerol Using Doped Graphenes as Metal-Free Catalysts. *Green Chem.* **2017**, *19*, 3061.
(14) Esteve-Adell, I.; Bakker, N.; Primo, A.; Hensen, E. J. M.; García, H. Graphene as Metal-Free Catalyst for Aqueous Phase Reforming of Ethylene Glycol. *ChemistrySelect* **2017**, *2*, 6338.
(15) Huber, G. W.; Shabaker, J. W.; Evans, S. T.; Dumesic, J. A. Aqueous-Phase Reforming of Ethylene Glycol over Supported Pt and Pd Bimetallic Catalysts. *Appl. Catal., B* **2006**, *62*, 226.
(16) Nozawa, T.; Yoshida, A.; Hikichi, S.; Naito, S. Effects of Re Addition upon Aqueous Phase Reforming of Ethanol over TiO_2 Supported Rh and Ir Catalysts. *Int. J. Hydrogen Energy* **2015**, *40*, 4129.
(17) Davda, R. R.; Shabaker, J. W.; Huber, G. W.; Cortright, R. D.; Dumesic, J. A. Aqueous-Phase Reforming of Ethylene Glycol on Silica-Supported Metal Catalysts. *Appl. Catal., B* **2003**, *43*, 13.
(18) He, C.; Zheng, J.; Wang, K.; Lin, H.; Wang, J.-Y.; Yang, Y. Sorption Enhanced Aqueous Phase Reforming of Glycerol for Hydrogen Production over Pt-Ni Supported on Multi-Walled Carbon Nanotubes. *Appl. Catal., B* **2015**, *162*, 401.
(19) Kaya, B.; Irmak, S.; Hasanoğlu, A.; Erbatur, O. Developing Pt Based Bimetallic and Trimetallic Carbon Supported Catalysts for Aqueous-Phase Reforming of Biomass-Derived Compounds. *Int. J. Hydrogen Energy* **2015**, *40*, 3849.
(20) van Haasterecht, T.; Ludding, C. C. I.; de Jong, K. P.; Bitter, J. H. Stability and Activity of Carbon Nanofiber-Supported Catalysts in the Aqueous Phase Reforming of Ethylene Glycol. *J. Energy Chem.* **2013**, *22*, 257.
(21) Kunkes, E. L.; Soares, R. R.; Simonetti, D. A.; Dumesic, J. A. An Integrated Catalytic Approach for the Production of Hydrogen by Glycerol Reforming Coupled with Water-Gas Shift. *Appl. Catal., B* **2009**, *90*, 693.
(22) Wen, G.; Xu, Y.; Xu, Z.; Tian, Z. Direct Conversion of Cellulose into Hydrogen by Aqueous-Phase Reforming Process. *Catal. Commun.* **2010**, *11*, 522.
(23) Kim, H.-D.; Park, H. J.; Kim, T.-W.; Jeong, K.-E.; Chae, H.-J.; Jeong, S.-Y.; Lee, C.-H.; Kim, C.-U. Hydrogen Production through the Aqueous Phase Reforming of Ethylene Glycol over Supported Pt-Based Bimetallic Catalysts. *Int. J. Hydrogen Energy* **2012**, *37*, 8310.
(24) Zhang, J.; Lu, F.; Yu, W.; Chen, J.; Chen, S.; Gao, J.; Xu, J. Selective Hydrogenative Cleavage of C−C Bonds in Sorbitol Using Ni−Re/C Catalyst under Nitrogen Atmosphere. *Catal. Today* **2014**, *234*, 107.
(25) Otromke, M.; Theiss, L.; Wunsch, A.; Susdorf, A.; Aicher, T. Selective and Controllable Purification of Monomeric Lignin Model Compounds via Aqueous Phase Reforming. *Green Chem.* **2015**, *17*, 3621.
(26) Esteve-Adell, I.; Bakker, N.; Primo, A.; Hensen, E.; García, H. Oriented Pt Nanoparticles Supported on Few-Layers Graphene as Highly Active Catalyst for Aqueous-Phase Reforming of Ethylene Glycol. *ACS Appl. Mater. Interfaces* **2016**, *8*, 33690.
(27) Ciftci, A.; Ligthart, D. A. J. M.; Sen, A. O.; van Hoof, A. J. F.; Friedrich, H.; Hensen, E. J. M. Pt-Re Synergy in Aqueous-Phase Reforming of Glycerol and the Water-Gas Shift Reaction. *J. Catal.* **2014**, *311*, 88.
(28) D'Hondt, E.; Van de Vyver, S.; Sels, B. F.; Jacobs, P. A. Catalytic Glycerol Conversion into 1,2-Propanediol in Absence of Added Hydrogen. *Chem. Commun. (Cambridge, U. K.)* **2008**, 6011.
(29) Wei, Z.; Karim, A. M.; Li, Y.; King, D. L.; Wang, Y. Elucidation of the Roles of Re in Steam Reforming of Glycerol over Pt−Re/C Catalysts. *J. Catal.* **2015**, *322*, 49.
(30) Ciftci, A.; Ligthart, D. A. J. M.; Hensen, E. J. M. Influence of Pt Particle Size and Re Addition by Catalytic Reduction on Aqueous Phase Reforming of Glycerol for Carbon-Supported Pt(Re) Catalysts. *Appl. Catal., B* **2015**, *174−175*, 126.
(31) Bossola, F.; Pereira-Hernandez, X. I.; Evangelisti, C.; Wang, Y.; Dal Santo, V. Investigation of the Promoting Effect of Mn on a Pt/C Catalyst for the Steam and Aqueous Phase Reforming of Glycerol. *J. Catal.* **2017**, *349*, 75.
(32) Meryemoglu, B.; Irmak, S.; Hasanoglu, A.; Erbatur, O.; Kaya, B. Influence of Particle Size of Support on Reforming Activity and Selectivity of Activated Carbon Supported Platinum Catalyst in APR. *Fuel* **2014**, *134*, 354.
(33) Chang, A. C.-C.; Louh, R. F.; Wong, D.; Tseng, J.; Lee, Y. S. Hydrogen Production by Aqueous-Phase Biomass Reforming over Carbon Textile Supported Pt−Ru Bimetallic Catalysts. *Int. J. Hydrogen Energy* **2011**, *36*, 8794.
(34) Meryemoglu, B.; Hesenov, A.; Irmak, S.; Atanur, O. M.; Erbatur, O. Aqueous-Phase Reforming of Biomass Using Various Types of Supported Precious Metal and Raney-Nickel Catalysts for Hydrogen Production. *Int. J. Hydrogen Energy* **2010**, *35*, 12580.
(35) Kaya, B.; Irmak, S.; Hasanoglu, A.; Erbatur, O. Evaluation of Various Carbon Materials Supported Pt Catalyts for Aqueous-Phase Reforming of Lignocellulosic Biomass Hydrolysate. *Int. J. Hydrogen Energy* **2014**, *39*, 10135.
(36) Meryemoglu, B.; Irmak, S.; Hasanoglu, A. Production of Activated Carbon Materials from Kenaf Biomass to Be Used as Catalyst Support in Aqueous-Phase Reforming Process. *Fuel Process. Technol.* **2016**, *151*, 59.
(37) van Haasterecht, T.; Ludding, C. C. I.; de Jong, K. P.; Bitter, J. H. Toward Stable Nickel Catalysts for Aqueous Phase Reforming of Biomass-Derived Feedstock under Reducing and Alkaline Conditions. *J. Catal.* **2014**, *319*, 27.
(38) Wang, X.; Li, N.; Zhang, Z.; Wang, C.; Pfefferle, L. D.; Haller, G. L. High-Yield Hydrogen Production from Aqueous Phase Reforming over Single-Walled Carbon Nanotube Supported Catalysts. *ACS Catal.* **2012**, *2*, 1480.
(39) Wang, X.; Li, N.; Pfefferle, L. D.; Haller, G. L. Pt−Co Bimetallic Catalyst Supported on Single Walled Carbon Nanotube: XAS and Aqueous Phase Reforming Activity Studies. *Catal. Today* **2009**, *146*, 160.
(40) Shabaker, J. W.; Huber, G. W.; Davda, R. R.; Cortright, R. D.; Dumesic, J. A. Aqueous-Phase Reforming of Ethylene Glycol over Supported Platinum Catalysts. *Catal. Lett.* **2003**, *88*, 1.
(41) Kim, T.-W.; Kim, H.-D.; Jeong, K.-E.; Chae, H.-J.; Jeong, S.-Y.; Lee, C.-H.; Kim, C.-U. Catalytic Production of Hydrogen through Aqueous-Phase Reforming over Platinum/ordered Mesoporous Carbon Catalysts. *Green Chem.* **2011**, *13*, 1718.
(42) Wang, X.; Li, N.; Pfefferle, L. D.; Haller, G. L. Pt−Co Bimetallic Catalyst Supported on Single-Walled Carbon Nanotubes: Effect of Alloy Formation and Oxygen Containing Groups. *J. Phys. Chem. C* **2010**, *114*, 16996.

DOI: 10.1021/acs.iecr.7b04937
Ind. Eng. Chem. Res. 2018, 57, 2050−2067

(43) Wang, X.; Li, N.; Webb, J. A.; Pfefferle, L. D.; Haller, G. L. Effect of Surface Oxygen Containing Groups on the Catalytic Activity of Multi-Walled Carbon Nanotube Supported Pt Catalyst. *Appl. Catal., B* **2010**, *101*, 21.
(44) Kim, H.-D.; Park, H. J.; Kim, T.-W.; Jeong, K.-E.; Chae, H.-J.; Jeong, S.-Y.; Lee, C.-H.; Kim, C.-U. The Effect of Support and Reaction Conditions on Aqueous Phase Reforming of Polyol over Supported Pt−Re Bimetallic Catalysts. *Catal. Today* **2012**, *185*, 73.
(45) Jeong, K. E.; Kim, H. D.; Kim, T. W.; Kim, J. W.; Chae, H. J.; Jeong, S. Y.; Kim, C. U. Hydrogen Production by Aqueous Phase Reforming of Polyols over Nano- and Micro-Sized Mesoporous Carbon Supported Platinum Catalysts. *Catal. Today* **2014**, *232*, 151.
(46) Kunkes, E. L.; Simonetti, D. A.; Dumesic, J. A.; Pyrz, W. D.; Murillo, L. E.; Chen, J. G.; Buttrey, D. J. The Role of Rhenium in the Conversion of Glycerol to Synthesis Gas over Carbon Supported Platinum−rhenium Catalysts. *J. Catal.* **2008**, *260*, 164.
(47) Wen, G.; Xu, Y.; Ma, H.; Xu, Z.; Tian, Z. Production of Hydrogen by Aqueous-Phase Reforming of Glycerol. *Int. J. Hydrogen Energy* **2008**, *33*, 6657.
(48) Dietrich, P. J.; Sollberger, F. G.; Akatay, M. C.; Stach, E. A.; Delgass, W. N.; Miller, J. T.; Ribeiro, F. H. Structural and Catalytic Differences in the Effect of Co and Mo as Promoters for Pt-Based Aqueous Phase Reforming Catalysts. *Appl. Catal., B* **2014**, *156−157*, 236.
(49) Kim, T.-W.; Park, H. J.; Yang, Y.-C.; Jeong, S.-Y.; Kim, C.-U. Hydrogen Production via the Aqueous Phase Reforming of Polyols over Three Dimensionally Mesoporous Carbon Supported Catalysts. *Int. J. Hydrogen Energy* **2014**, *39*, 11509.
(50) Kirilin, A. V.; Hasse, B.; Tokarev, A. V.; Kustov, L. M.; Baeva, G. N.; Bragina, G. O.; Stakheev, A. Y.; Rautio, A.-R.; Salmi, T.; Etzold, B. J. M.; Mikkola, J.-P.; Murzin, D.Yu. Aqueous-Phase Reforming of Xylitol over Pt/C and Pt/TiC-CDC Catalysts: Catalyst Characterization and Catalytic Performance. *Catal. Sci. Technol.* **2014**, *4*, 387.
(51) Neira D'Angelo, M. F.; Ordomsky, V.; van der Schaaf, J.; Schouten, J. C.; Nijhuis, T. A. Selective Production of Methane from Aqueous Biocarbohydrate Streams over a Mixture of Platinum and Ruthenium Catalysts. *ChemSusChem* **2014**, *7*, 627.
(52) Park, H. J.; Kim, H.-D.; Kim, T.-W.; Jeong, K.-E.; Chae, H.-J.; Jeong, S.-Y.; Chung, Y.-M.; Park, Y.-K.; Kim, C.-U. Production of Biohydrogen by Aqueous Phase Reforming of Polyols over Platinum Catalysts Supported on Three-Dimensionally Bimodal Mesoporous Carbon. *ChemSusChem* **2012**, *5*, 629.
(53) Boga, D. A.; Liu, F.; Bruijnincx, P. C. A.; Weckhuysen, B. M. Aqueous-Phase Reforming of Crude Glycerol: Effect of Impurities on Hydrogen Production. *Catal. Sci. Technol.* **2016**, *6*, 134.
(54) Zhang, L.; Karim, A. M.; Engelhard, M. H.; Wei, Z.; King, D. L.; Wang, Y. Correlation of Pt−Re Surface Properties with Reaction Pathways for the Aqueous-Phase Reforming of Glycerol. *J. Catal.* **2012**, *287*, 37.
(55) King, D. L.; Zhang, L.; Xia, G.; Karim, A. M.; Heldebrant, D. J.; Wang, X.; Peterson, T.; Wang, Y. Aqueous Phase Reforming of Glycerol for Hydrogen Production over Pt−Re Supported on Carbon. *Appl. Catal., B* **2010**, *99*, 206.
(56) Ciftci, A.; Ligthart, D. A. J. M.; Hensen, E. J. M. Aqueous Phase Reforming of Glycerol over Re-Promoted Pt and Rh Catalysts. *Green Chem.* **2014**, *16*, 853.
(57) Fu, J.; Hakim, S. H.; Shanks, B. H. Aqueous-Phase Processing of Bio-Oil Model Compounds over Pt−Re Supported on Carbon. *Top. Catal.* **2012**, *55*, 140.
(58) Kim, D.; Vardon, D. R.; Murali, D.; Sharma, B. K.; Strathmann, T. J. Valorization of Waste Lipids through Hydrothermal Catalytic Conversion to Liquid Hydrocarbon Fuels with in Situ Hydrogen Production. *ACS Sustainable Chem. Eng.* **2016**, *4*, 1775.
(59) de Vlieger, D. J. M.; Lefferts, L.; Seshan, K. Ru Decorated Carbon Nanotubes − a Promising Catalyst for Reforming Bio-Based Acetic Acid in the Aqueous Phase. *Green Chem.* **2014**, *16*, 864.
(60) Rahman, M. M. H_2 Production from Aqueous-Phase Reforming of Glycerol over Cu-Ni Bimetallic Catalysts Supported on Carbon Nanotubes. *Int. J. Hydrogen Energy* **2015**, *40*, 14833.
(61) Dietrich, P. J.; Akatay, M. C.; Sollberger, F. G.; Stach, E. A.; Miller, T.; Delgass, W. N.; Ribeiro, F. H. Effect of Co Loading on the Activity and Selectivity of PtCo Aqueous Phase Reforming Catalysts. *ACS Catal.* **2014**, *4*, 480.
(62) Manfro, R. L.; da Costa, A. F.; Ribeiro, N. F. P.; Souza, M. M. V. M Hydrogen Production by Aqueous-Phase Reforming of Glycerol over Nickel Catalysts Supported on CeO_2. *Fuel Process. Technol.* **2011**, *92*, 330.
(63) Shabaker, J. W.; Huber, G. W.; Dumesic, J. A. Aqueous-Phase Reforming of Oxygenated Hydrocarbons over Sn-Modified Ni Catalysts. *J. Catal.* **2004**, *222*, 180.
(64) Shabaker, J. W.; Simonetti, D. A.; Cortright, R. D.; Dumesic, J. A. Sn-Modified Ni Catalysts for Aqueous-Phase Reforming: Characterization and Deactivation Studies. *J. Catal.* **2005**, *231*, 67.
(65) Pienaar, A. D.; de Klerk, A. Nickel Catalyst Stability toward Carboxylic Acids. *Ind. Eng. Chem. Res.* **2008**, *47*, 4962.
(66) El Doukkali, M.; Iriondo, A.; Arias, P. L.; Requies, J.; Gandarías, I.; Jalowiecki-Duhamel, L.; Dumeignil, F. A Comparison of Sol−gel and Impregnated Pt or/and Ni Based γ-Alumina Catalysts for Bioglycerol Aqueous Phase Reforming. *Appl. Catal., B* **2012**, *125*, 516.
(67) Jiang, T.; Zhang, Q.; Wang, T.-J.; Zhang, Q.; Ma, L.-L. High Yield of Pentane Production by Aqueous-Phase Reforming of Xylitol over Ni/HZSM-5 and Ni/MCM22 Catalysts. *Energy Convers. Manage.* **2012**, *59*, 58.
(68) Jiang, T.; Wang, T.; Ma, L.; Li, Y.; Zhang, Q.; Zhang, X. Investigation on the Xylitol Aqueous-Phase Reforming Performance for Pentane Production over Pt/HZSM-5 and Ni/HZSM-5 Catalysts. *Appl. Energy* **2012**, *90*, 51.
(69) Liu, J.; Sun, B.; Hu, J.; Pei, Y.; Li, H.; Qiao, M. Aqueous-Phase Reforming of Ethylene Glycol to Hydrogen on Pd/Fe_3O_4 Catalyst Prepared by Co-Precipitation: Metal−support Interaction and Excellent Intrinsic Activity. *J. Catal.* **2010**, *274*, 287.
(70) Menezes, A. O.; Rodrigues, M. T.; Zimmaro, A.; Borges, L. E. P.; Fraga, M. A. Production of Renewable Hydrogen from Aqueous-Phase Reforming of Glycerol over Pt Catalysts Supported on Different Oxides. *Renewable Energy* **2011**, *36*, 595.
(71) Ma, J. Q.; Xu, Y.; Xu, Y. F.; Li, H.; Li, H. X.; Li, P.; Zhou, X. G. Aqueous-Phase Reforming of Ethylene Glycol to Hydrogen on Supported Pt Catalysts. *Adv. Mater. Res.* **2011**, *347−353*, 2511.
(72) Guo, Y.; Azmat, M. U.; Liu, X.; Wang, Y.; Lu, G. Effect of Support's Basic Properties on Hydrogen Production in Aqueous-Phase Reforming of Glycerol and Correlation between WGS and APR. *Appl. Energy* **2012**, *92*, 218.
(73) Murzin, D. Yu.; Garcia, S.; Russo, V.; Kilpiö, T. T.; Godina, L. I.; Tokarev, A.; Kirilin, A.; Simakova, I. L.; Poulston, S.; Sladkovskiy, D. A.; Wärnå, J. Kinetics, Modelling and Process Design of Hydrogen Production by Aqueous Phase Reforming of Xylitol. *Ind. Eng. Chem. Res.* **2017**, *56*, 13240.
(74) Scofield, J. H. Hartree-Slater Subshell Photoionization Cross-Sections at 1254 and 1487 eV. *J. Electron Spectrosc. Relat. Phenom.* **1976**, *8*, 129.
(75) Bergeret, G.; Gallezot, P. Particle Size and Dispersion Measurement. *Handb. Heterog. Catal.* **2002**, 738.
(76) Torrente-Murciano, L. The Importance of Particle-Support Interaction on Particle Size Determination by Gas Chemisorption. *J. Nanopart. Res.* **2016**, *18*, 1.
(77) Abotsi, G. M. K.; Scaroni, A. W. A Review of Carbon-Supported Hydrodesulfurization Catalysts. *Fuel Process. Technol.* **1989**, *22*, 107.
(78) Perry, R.; Green, D.; Maloney, J. *Perry's Chemical Engineers' Handbook*; The McGraw- Hill Companies: New York, 1997.
(79) Reid, R. C.; Prausnitz, J. M.; Sherwood, T. K. *The Properties of Gases and Liquids*, 3rd ed.; McGraw-Hill: New York, 1977.
(80) Le Bas, G. *The Molecular Volumes of Liquid Chemical Compounds*; Longmans, Green: New York, 1915.
(81) Sie, S. T.; Krishna, R. Process Development and Scale up: III. Scale-up and Scale-down of Trickle Bed Processes. *Rev. Chem. Eng.* **1998**, *14*, 203.
(82) Saroha, A. K.; Nigam, K. D. P. Trickle Bed Reactors. *Rev. Chem. Eng.* **1996**, *12*, 207.

DOI: 10.1021/acs.iecr.7b04937
Ind. Eng. Chem. Res. 2018, 57, 2050−2067

(83) Barbelli, M. L.; Pompeo, F.; Santori, G. F.; Nichio, N. N. Pt Catalyst Supported on α-Al_2O_3 Modified with CeO_2 and ZrO_2 for Aqueous-Phase-Reforming of Glycerol. *Catal. Today* **2013**, *213*, 58.
(84) Lehnert, K.; Claus, P. Influence of Pt Particle Size and Support Type on the Aqueous-Phase Reforming of Glycerol. *Catal. Commun.* **2008**, *9*, 2543.
(85) Chen, A.; Chen, P.; Cao, D.; Lou, H. Aqueous-Phase Reforming of the Low-Boiling Fraction of Bio-Oil for Hydrogen Production: The Size Effect of Pt/Al_2O_3. *Int. J. Hydrogen Energy* **2015**, *40*, 14798.
(86) Simonetti, D. A.; Kunkes, E. L.; Dumesic, J. A. Gas-Phase Conversion of Glycerol to Synthesis Gas over Carbon-Supported Platinum and Platinum−rhenium Catalysts. *J. Catal.* **2007**, *247*, 298.
(87) Godina, L. I.; Kirilin, A. V.; Tokarev, A. V.; Murzin, D. Yu. Aqueous Phase Reforming of Industrially Relevant Sugar Alcohols with Different Chirality. *ACS Catal.* **2015**, *5*, 2989.
(88) Huber, G. W.; Cortright, R. D.; Dumesic, J. A. Renewable Alkanes by Aqueous-Phase Reforming of Biomass-Derived Oxygenates. *Angew. Chem., Int. Ed.* **2004**, *43*, 1549.
(89) Godina, L. I.; Tokarev, A. V.; Simakova, I. L.; Mäki-Arvela, P.; Kortesmäki, E.; Gläsel, J.; Kronberg, L.; Etzold, B.; Murzin, D. Yu. Aqueous-Phase Reforming of Alcohols with Three Carbon Atoms on Carbon- Supported Pt. *Catal. Today* **2018**, *301*, 78.
(90) Kirilin, A.; Wärnå, J.; Tokarev, A.; Murzin, D. Yu. Kinetic Modeling of Sorbitol Aqueous-Phase Reforming over Pt/Al_2O_3. *Ind. Eng. Chem. Res.* **2014**, *53*, 4580.
(91) Kirilin, A. V.; Tokarev, A. V.; Murzina, E. V.; Kustov, L. M.; Mikkola, J.-P.; Murzin, D. Yu. Reaction Products and Transformations of Intermediates in the Aqueous-Phase Reforming of Sorbitol. *ChemSusChem* **2010**, *3*, 708.

DOI: 10.1021/acs.iecr.7b04937
Ind. Eng. Chem. Res. 2018, 57, 2050−2067